

1 Temporal and genetic link between incremental pluton assembly  
2 and pulsed porphyry Cu-Mo formation in accretionary orogens

3 **Hervé Rezeau<sup>1,\*</sup>, Robert Moritz<sup>1</sup>, Jörn-Frederik Wotzlaw<sup>2</sup>, Rodrik Tayan<sup>3,†</sup>, Rafael**  
4 **Melkonyan<sup>3</sup>, Alexey Ulianov<sup>4</sup>, David Selby<sup>5</sup>, François-Xavier d'Abzac<sup>1</sup> and Richard A.**  
5 **Stern<sup>6</sup>**

6 <sup>1</sup>Department of Earth Sciences, University of Geneva, 1205 Geneva, Switzerland

7 <sup>2</sup>Institute of Geochemistry and Petrology, ETH Zurich, 8092 Zurich, Switzerland

8 <sup>3</sup>Institute of Geological Sciences, National Academy of Sciences, 0019 Yerevan, Armenia

9 <sup>4</sup>Institute of Earth Sciences, University of Lausanne, 1015 Lausanne, Switzerland

10 <sup>5</sup>Department of Earth Sciences, University of Durham, DH1 3LE Durham, United Kingdom

11 <sup>6</sup>Canadian Centre for Isotopic Microanalysis, University of Alberta, Edmonton, Canada

12 \*corresponding author: herve.rezeau@unige.ch

13 †deceased March 25<sup>th</sup> 2016

14

15 **ABSTRACT**

16 Economically important porphyry Cu-Mo deposits (PCDs) are generally hosted by upper crustal  
17 plutons of variable chemical compositions related to distinct geodynamic settings. The absolute  
18 timing and duration of pluton assembly and PCD formation is critical to understand the genetic  
19 relationship between these interrelated processes. Here we present new comprehensive zircon U-  
20 Pb and molybdenite Re-Os ages that tightly constrain the timing and duration of pluton assembly  
21 and the age of mineralization in one of the largest ore-bearing plutons of the central Tethyan  
22 metallogenic belt, the Meghri-Ordubad pluton, southern Armenia and Nakhitchevan, Lesser

23 Caucasus. This composite pluton was incrementally assembled during three compositionally  
24 distinct magmatic episodes over about 30 m.y., comprising Middle Eocene (48.9-43.1 Ma) calc-  
25 alkaline subduction-related magmatism lasting  $5.8 \pm 0.8$  m.y., followed by post-subduction Late  
26 Eocene - Middle Oligocene (37.8-28.1 Ma) shoshonitic magmatism over  $9.7 \pm 0.9$  m.y, and Late  
27 Oligocene - Early Miocene (26.6-21.2 Ma) adakitic magmatism consisting of shoshonitic dikes  
28 and high-K calc-alkaline granodioritic magmas emplaced over  $5.4 \pm 0.4$  m.y. Despite the distinct  
29 geodynamic settings and magma compositions, each intrusive suite culminated in the formation  
30 of variably sized PCDs, including the giant Oligocene Kadjaran porphyry Cu-Mo deposit  
31 associated with high Sr/Y shoshonitic magmas. Complementary *in-situ* zircon hafnium ( $\epsilon\text{Hf}_{\text{zircon}}$   
32 = +8 to +11.3) and oxygen ( $\delta^{18}\text{O}_{\text{zircon}} = +4.6$  to +6.0 ‰) isotope data support a mantle-dominated  
33 magma source with limited crustal contribution and/or cannibalization of young and juvenile  
34 lower crustal cumulates. We conclude that, independently of geodynamic setting and magma  
35 composition, long-lived (5-10 m.y.) incremental mantle-derived magmatism is a pre-requisite to  
36 form fertile magmatic-hydrothermal systems, and especially giant PCDs.

37

## 38 INTRODUCTION

39 The majority of porphyry Cu-Mo deposits (PCDs) are associated with subduction-related calc-  
40 alkaline upper-crustal plutons (Sillitoe, 2010). However, porphyry Cu-Mo systems have recently  
41 also been recognized in post-subduction settings, particularly along the Tethyan metallogenic  
42 belt (e.g., Richards, 2015; Hou et al., 2015a, b; Moritz et al., 2016). This raises a number of  
43 questions concerning the primary control on PCD formation, as most models require active  
44 oceanic subduction to generate large volumes of hydrous, oxidized, S-rich, and Cu-rich magmas  
45 derived from a subcontinental lithospheric mantle metasomatized by slab fluids, and repeated

46 mafic magma injections to provide sulfur, metals and volatiles into upper crustal reservoirs (e.g.,  
47 Hattori and Keith, 2001; Scaillet, 2010; Audétat and Simon, 2012; Tapster et al., 2016). Ore-  
48 forming processes in PCDs occur over short timescales of  $<10^3$  to  $10^4$  years (e.g., von Quadt et  
49 al., 2011; Chiaradia et al., 2013), which are in marked contrast to the duration of incremental  
50 assembly of the host plutons lasting  $10^5$  to  $10^6$  years (Rohrlach and Loucks, 2005; Chelle-  
51 Michou et al., 2014; Correa et al., 2016). In most magmatic-hydrothermal systems, ore formation  
52 occurs late in the magmatic evolution (e.g., Sillitoe, 2010; Audétat and Simon, 2012), but the  
53 precise temporal and genetic relationships between the entire pluton construction and PCD  
54 formation remains poorly documented.

55 Recently, Moritz et al. (2016) documented the regional tectonic evolution of the southernmost  
56 Lesser Caucasus from a subduction to post-collisional setting with coeval mineralization pulses,  
57 however the absolute temporal link between intrusions and PCDs remained elusive due to  
58 limited geochronological data. Here we investigate the absolute temporal relationship between  
59 incremental pluton construction and PCD formation using a large data set of new zircon U-Pb  
60 and molybdenite Re-Os data from one of the largest ore-bearing plutons of the central Tethyan  
61 metallogenic belt, the Meghri-Ordubad pluton (MOP) in southern Armenia and Nakhitchevan,  
62 Lesser Caucasus. The MOP comprises three long-lived intrusive suites, which culminated in the  
63 formation of variably sized PCDs, including the giant Oligocene Kadjaran PCD (Figs. 1 and 2).  
64 Our comprehensive U-Pb and Re-Os geochronological framework documents in detail the  
65 incremental construction of the MOP over 30 m.y. and the timing of ore formation allowing  
66 improved understanding of the conditions and processes required to form PCDs. Complementary  
67 *in-situ* zircon hafnium and oxygen isotope data are used to estimate mantle and crustal  
68 contributions to the ore-forming magmas.

69

## 70 **GEOLOGICAL SETTING AND ANALYTICAL METHODS**

71 The ore-bearing MOP belongs to the regional fertile Cenozoic magmatic belt extending from  
72 Turkey to Iran that formed during the final convergence and collision of the Arabian and  
73 Eurasian plates (Fig. DR1). The MOP represents the largest composite intrusion of the Lesser  
74 Caucasus (800 km<sup>2</sup>) and intrudes a thick sequence of Cenozoic terrigenous sedimentary and  
75 subalkaline to calc-alkaline basaltic to andesitic volcanic rocks (Karamyan et al., 1974). The  
76 MOP is the result of a long-lasting Middle Eocene to Early Miocene evolution, including  
77 subduction-related calc-alkaline magmatism followed by post-subduction shoshonitic to high-K  
78 calc-alkaline magmatism (Figs. 1A and DR2; Moritz et al., 2016). The MOP is bordered by two  
79 regional NNW-oriented faults with both vertical and dextral strike-slip movements, and another  
80 parallel fault extends through its central part and controls the location of PCDs (Fig. 2; Tayan,  
81 1998).

82 New zircon U-Pb ages were obtained by laser ablation inductively coupled plasma mass  
83 spectrometry (LA-ICP-MS) from thirty representative magmatic rock samples covering the  
84 entire temporal and compositional range of the MOP. Nine molybdenite Re-Os ages were  
85 obtained by isotope dilution negative thermal ionization mass spectrometry (ID-N-TIMS) from  
86 mineralization events associated with all three magmatic episodes. *In-situ* multiple collector  
87 inductively coupled plasma mass spectrometry (MC-ICP-MS) hafnium and secondary ion mass  
88 spectrometry (SIMS) oxygen isotope data were obtained on selected zircon grains. The complete  
89 analytical details and data set, together with a summary of the geochemical composition of dated  
90 samples are provided in the data repository<sup>1</sup>.

91

## 92 INCREMENTAL PLUTON CONSTRUCTION

93 A total of 601 new LA-ICP-MS zircon U-Pb dates (Table DR2), together with previously  
94 published chemical abrasion isotope dilution thermal ionization mass spectrometry (CA-ID-  
95 TIMS) zircon U-Pb ages (Table DR1; Moritz et al., 2016), place tight spatial-temporal  
96 constraints on the MOP incremental assembly (Figs. 1A and 2).

97 In the southern part of the MOP (Fig. 2), the subduction-related calc-alkaline magmatism starts  
98 with two granitic and tonalitic intrusions at  $48.9 \pm 0.6$  and  $47.6 \pm 0.6$  Ma, followed by gabbro-  
99 diorite-tonalite-granodiorite intrusions and NNW-oriented basaltic andesite dikes emplaced  
100 between  $45.9 \pm 0.9$  and  $43.8 \pm 0.6$  Ma (Fig. 1A). These ages are in agreement with CA-ID-TIMS  
101 ages from similar samples (Fig. 1A; Table DR1). In the northern part of the MOP (Fig. 2), a  
102 monzodiorite is intruded by a tonalite and yield slightly younger U-Pb ages of  $42.9 \pm 0.5$  and  
103  $43.1 \pm 0.5$  Ma, respectively (Fig. 1A). The Middle Eocene intrusive suite documents  $5.8 \pm 0.8$   
104 m.y. of incremental magmatism.

105 Following a magmatic lull of  $5.1 \pm 0.9$  m.y., pluton assembly resumed with emplacement of  
106 post-subduction high Sr/Y shoshonitic intrusions (Fig. 1A). In the southeastern part of the MOP  
107 (Fig. 2), a monzogabbro and a monzodiorite yield indistinguishable ages of  $37.8 \pm 0.8$  and  $37.0 \pm$   
108  $0.4$  Ma, respectively (Fig. 1A). Further north along the Vank-Kaler road and along the Meghri  
109 ridge (Fig. 2), five monzogabbroic-monzodioritic intrusions were emplaced between  $35.7 \pm 0.6$   
110 and  $33.5 \pm 0.6$  Ma, and are crosscut by trachyandesitic and syenitic dikes that yield ages of  $33.7$   
111  $\pm 0.5$  and  $33.6 \pm 0.6$  Ma, respectively (Fig. 1A). Along the Meghri ridge, a hornblende gabbro  
112 was dated at  $33.43 \pm 0.02$  Ma by CA-ID-TIMS (Fig. 1A; Table DR1). Further north and west  
113 (Fig. 2), the Kadjaran ore field exposes a monzonite with an age of  $31.9 \pm 0.5$  Ma, which is in  
114 agreement with a CA-ID-TIMS U-Pb age of  $31.83 \pm 0.02$  Ma, and crosscut by a syenitic sill

115 dated at  $31.1 \pm 0.5$  Ma (Fig. 1A; Table DR1). Younger monzonite and monzogabbro were  
116 emplaced at  $28.3 \pm 0.4$  and  $28.1 \pm 0.4$  Ma, respectively. The entire Late Eocene to Middle  
117 Oligocene intrusive suite comprises  $9.7 \pm 0.9$  m.y. of episodic magmatism.  
118 In the Kadjaran ore field (Fig. 2), the post-subduction magmatism continued with the  
119 emplacement of Late Oligocene NNW-oriented adakitic shoshonitic trachybasaltic and  
120 trachyandesitic dikes between  $26.6 \pm 0.3$  and  $24.3 \pm 0.3$  Ma (Fig. 1A). These dikes contain  
121 significantly older zircons reflecting recycling of Middle Eocene and Early Oligocene intrusions.  
122 A younger, voluminous Early Miocene adakitic high-K calc-alkaline porphyritic granodiorite  
123 dated at  $22.8 \pm 0.5$  Ma is coeval with EW-oriented porphyritic granodioritic and trachyandesitic  
124 dikes dated at  $22.2 \pm 0.3$  and  $21.2 \pm 0.3$  Ma, respectively (Figs. 1A and 2), and overlap with CA-  
125 ID-TIMS ages for similar samples (Fig. 1A; Table DR1). The entire Late Oligocene - Early  
126 Miocene magmatism represents a third magmatic episode lasting  $5.4 \pm 0.4$  m.y. This latest  
127 magmatic suite is characterized by an adakitic signature, and also higher Mg#, Cr and Ni  
128 contents, distinct from the Late Eocene - Middle Oligocene high Sr/Y shoshonitic intrusive suite  
129 (Fig. DR2; Table DR1).

130

### 131 **TIMING OF MINERALIZATION**

132 The PCDs are aligned along the central N-S-oriented Tashtun fault (Fig. 2), but they were  
133 formed at different times during the MOP construction. The small tonnage PCDs (10 to 40 Mt at  
134 0.2-0.5 % Cu and 0.03-0.04 % Mo) yield molybdenite Re-Os ages of  $44.23 \pm 0.22$  and  $42.62 \pm$   
135  $0.22$  Ma in the southern part of the MOP at Agarak and Aygedzor, respectively, and  $43.14 \pm 0.22$   
136 Ma in the northern part at Hanqasar (Figs. 1A and 2; Table DR3). These Re-Os ages are  
137 indistinguishable from the ages of the youngest Middle Eocene intrusions, which tightly

138 constrain their formation to the end of subduction-related calc-alkaline magmatism (Fig. 1A).  
139 Molybdenite Re-Os dates reveal two distinct Cu-Mo mineralizing events in the giant Kadjaran  
140 PCD (2244 Mt at 0.2 % Cu and 0.02 % Mo). Molybdenite from the first mineralization event  
141 yields Re-Os ages between  $27.28 \pm 0.14$  and  $26.43 \pm 0.13$  Ma (Table DR3). This mineralization  
142 is hosted by the youngest Late Eocene - Middle Oligocene shoshonitic high Sr/Y intrusions and  
143 is crosscut by the oldest Late Oligocene shoshonitic adakitic mafic dike (Figs. 1A and DR3A).  
144 Therefore, the first mineralizing event in Kadjaran is attributed to the very end of the Late  
145 Eocene - Middle Oligocene post-subduction shoshonitic high Sr/Y magmatism. These ages are in  
146 agreement with Re-Os ages reported from the Iranian side of the MOP, namely the Qaradagh  
147 pluton (Simmonds and Moazzen, 2015).

148 A younger molybdenite Re-Os age of  $20.48 \pm 0.10$  Ma reveals a second ore-forming event in  
149 Kadjaran associated with a reopening of the structures hosting the 26-27 Ma-old Cu-Mo  
150 mineralization. It documents a genetic link with the Early Miocene adakitic high-K calc-alkaline  
151 porphyry granodiorite intrusion event (Fig. 1A; Table DR3), and supports a cogenetic link with  
152 Cu-rich epithermal veins overprinting porphyritic granodioritic dikes dated at  $22.2 \pm 0.3$  (Fig.  
153 DR3B). The Early Miocene hydrothermal event was already documented by a sericite K-Ar date  
154 of  $22 \pm 2$  Ma in Kadjaran (Bagdasaryan et al., 1969), and it is consistent with a molybdenite Re-  
155 Os age of  $21.01 \pm 0.15$  Ma reported from the Sungun PCD, located 70 km further south in  
156 northernmost Iran (Aghazadeh et al., 2015).

157 Placing all these Re-Os ages into our comprehensive U-Pb geochronology framework of  
158 incremental pluton construction clearly links PCDs formation to the latest stage of each intrusive  
159 suite (Fig. 1A).

160

161 **ASSESSING THE SOURCES OF ORE-FORMING MAGMAS USING HAFNIUM AND**  
162 **OXYGEN ISOTOPES**

163 Combined hafnium and oxygen isotopic signatures are powerful tools to trace the sources of  
164 magmas and place constraints on mantle and crustal contributions. Zircons from the MOP  
165 intrusive suites display median initial  $\epsilon_{\text{Hf}}$  values between +8.0 and +11.3, which suggest an  
166 overall predominance of mantle-derived magmas with limited crustal assimilation (Fig. 1B;  
167 Table DR3). This limited range in Hf isotopic compositions is in marked contrast with the  
168 significant differences in whole-rock geochemistry over about 30 m.y. (Fig. DR2; Table DR1).  
169 Interestingly, towards the end of the Middle Eocene calc-alkaline magmatism and throughout the  
170 Late Eocene to Early Miocene intrusive suites, Hf isotopic signatures become progressively  
171 more juvenile (Fig. 1B). Zircon oxygen isotope analyses reveal homogeneous  $\delta^{18}\text{O}$  values in  
172 individual rocks and crystals (Table DR4), but display a subtle  $\delta^{18}\text{O}$  increase from  $+5.20 \pm 0.19$   
173 ‰ to  $+5.97 \pm 0.22$  ‰ over 30 m.y. (Fig. 1B). These values and pattern imply very limited  
174 assimilation of supracrustal rocks (e.g., Lackey et al., 2005), and no crustal recycling of  
175 hydrothermally altered rocks (e.g., Bindeman, 2008). A single Middle Eocene sample with a  
176 median  $\delta^{18}\text{O}$  value of  $+4.51 \pm 0.69$  ‰ may be attributed to minor assimilation of altered shallow  
177 crustal material (Fig. 1B). The slight, but systematic and coeval increase of  $\delta^{18}\text{O}$  and  $\epsilon_{\text{Hf}}$  values  
178 over time together with the overall limited variations support a predominance of mantle-derived  
179 magmas with decreasing crustal contribution. It is consistent with a long-lived homogeneous  
180 deep reservoir in the lower crust or lithospheric mantle. Alternatively, this isotope pattern may be  
181 attributed to progressive cannibalization of young and juvenile lower crust, formed by mantle-  
182 derived magmas. However, this process cannot be quantified due to the limited isotopic contrast.

183



## 184 **CONTROLLING FACTORS OF PCD FORMATION**

185 The MOP represents a unique place to investigate controlling factors leading to the formation of  
186 PCDs because all three intrusive suites share similar duration of magmatic activity, isotopic  
187 signatures and local structural setting (Figs. 1 and 2), but they were emplaced under different  
188 geodynamic settings (subduction vs. post-subduction), and they are distinct with respect to their  
189 magma composition (Fig. DR2; Table DR1).

190 Our results suggest that protracted magmatism is a key pre-requisite for PCD genesis, and that  
191 differences in geodynamic setting and magma chemistry may account for modulating deposit  
192 tonnage. Caricchi et al. (2014) argued that for a similar magma flux, the duration of magmatism  
193 is one of the key differences between barren and ore-bearing plutons, but their dataset only  
194 included small-volume, short-lived barren plutons (Lago della Vacca and Torres del Paine).  
195 Meanwhile, long-lived plutonic systems with variable magma chemistry and related to different  
196 geodynamic settings are either barren at the present-day erosion level (e.g., Tuolumne intrusive  
197 suite; Coleman et al., 2004) or host variably sized PCDs, including giant deposits (e.g., Bingham  
198 vs. Corrocohuayco vs. El Abra; e.g., von Quadt et al., 2011; Chelle Michou et al., 2014; Correa  
199 et al., 2016).

200 In the MOP, Cu-Mo deposits of variable size were all formed at the end of long-lived magmatic  
201 episodes with durations between 5.4 and 9.7 m.y. (Fig. 1A). Therefore, we propose that while  
202 long-lived magmatism is required for PCD formation, the size of the PCDs may be modulated by  
203 the frequency of repeated injections of hot, hydrous, oxidized, S-rich, and Cu-rich mafic magmas  
204 that rejuvenate the upper crustal reservoir, allowing for the accumulation of sulfur, metals and  
205 volatiles in the upper crust (e.g., Hattori and Keith, 2001; Scaillet, 2010; Audétat and Simon,  
206 2012; Tapster et al., 2016).

207

208 **SUMMARY AND CONCLUSIONS**

209 This study documents 30 m.y. of incremental pluton construction in the central Tethyan  
210 metallogenic belt emplaced during a subduction to post-subduction geodynamic evolution. New  
211 comprehensive zircon U-Pb combined with molybdenite Re-Os geochronology in the MOP  
212 clearly links Cu-Mo mineralization to the late stages of three successive long-lived (5 to 10 m.y.)  
213 intrusive episodes. According to this study, various geodynamic settings and magmas of variable  
214 composition can produce PCDs, but the exploration challenge remains in identifying single long-  
215 lived and incrementally assembled magmatic suites associated with prospective ore zones. We  
216 conclude that protracted incremental crustal scale magmatism is a key requirement for the  
217 formation of PCDs in fertile magmatic belts, and that the frequency of upper crustal reservoir  
218 rejuvenation by mafic magmas may play a fundamental role for modulating PCD tonnage.

219

220 **ACKNOWLEDGEMENTS**

221 H.R. and R.M. acknowledge funding by the Swiss NSF projects 200020-138130 and 200020-  
222 155928, and the SCOPES Joint Research Project IZ73Z0-128324. Fieldwork of H.R. was funded  
223 by the Augustin Lombard Foundation of the Geneva SPHN Society and a SEG student grant  
224 from H.E. McKinstry Fund. J.F.W. acknowledges funding through the ETH Zurich postdoctoral  
225 fellowship program. We thank C. Chelle-Michou and S. Hovakimyan for fruitful discussions.  
226 Constructive comments by journal editor J. B. Murphy and reviews from Y. Lu, R.G. Lee and an  
227 anonymous reviewer improved the manuscript. This paper is dedicated to the memory of Rodrik  
228 Tayan, who spent his life studying the Meghri pluton and shared his knowledge with passion.

229

230 **REFERENCES CITED**

- 231 Aghazadeh, M., Hou, Z., Badrzadeh, Z., and Zhou, L., 2015, Temporal–spatial distribution and  
232 tectonic setting of porphyry copper deposits in Iran: Constraints from zircon U–Pb and  
233 molybdenite Re–Os geochronology: *Ore Geology Reviews*, v. 70, p.385-406, doi:  
234 10.1016/j.oregeorev.2015.03.003.
- 235 Audétat, A., and Simon, A.C., 2012, Magmatic controls on porphyry Cu genesis, *in* Hedenquist,  
236 J.W., Harris, M., and Camus, F., eds, *Geology and Genesis of Major Copper Deposits*  
237 *and Districts of the World: A Tribute to Richard Sillitoe*: Society of Economic  
238 Geologists, Special Publication 16, p. 553-572.
- 239 Bagdasaryan, G.P., Gukasyan, R.Kh., and Karamyan, K.A., 1969, Absolute dating of Armenian  
240 ore formations: *International Geology Review*, v. 11, p. 1166–1172, doi:  
241 10.1080/00206816909475161.
- 242 Bindeman, I., 2008, Oxygen isotopes in mantle and crustal magmas as revealed by single crystal  
243 analysis: *Reviews in Mineralogy and Geochemistry*, v. 69, p. 445-478, doi:  
244 10.2138/rmg.2008.69.12.
- 245 Caricchi, L., Simpson, G., and Schaltegger, U., 2014, Zircons reveal magma fluxes in the Earth’s  
246 crust: *Nature*, v. 511, p. 457-461, doi: 10.1038/nature13532.
- 247 Chelle-Michou, C., Chiaradia, M., Ovtcharova, M., Ulianov, A., and Wotzlaw, J.F., 2014, Zircon  
248 petrochronology reveals the temporal link between porphyry systems and the magmatic  
249 evolution of their hidden plutonic roots (the Eocene Corocchohuayco deposit, Peru):  
250 *Lithos*, v. 198, p. 129-140, doi: 10.1016/j.lithos.2014.03.017.
- 251 Chiaradia, M., Schaltegger, U., Spikings, R., Wotzlaw, J.F., and Ovtcharova, M., 2013, How  
252 accurately can we date the duration of magmatic-hydrothermal events in porphyry

253 systems? - An invited paper: *Economic Geology*, v. 108, p. 565-584, doi:  
254 10.2113/econgeo.108.4.565.

255 Coleman, D.S., Gray, W., and Glazner, A.F., 2004. Rethinking the emplacement and evolution  
256 of zoned plutons: Geochronologic evidence for incremental assembly of the Tuolumne  
257 Intrusive Suite, California: *Geology*, v. 32, p. 433-436, doi: 10.1130/G20220.1.

258 Correa, K.J., Rabbia, O.M., Hernández, L.B., Selby, D., and Astengo, M., 2016, The timing of  
259 magmatism and ore formation in the El Abra porphyry copper deposit, northern Chile:  
260 Implications for long-lived multiple-event magmatic-hydrothermal porphyry systems:  
261 *Economic Geology*, v. 111, p. 1-28, doi: 10.2113/econgeo.111.1.1.

262 Hattori, K.H., and Keith, J.D., 2001, Contribution of mafic melt to porphyry copper  
263 mineralization: evidence from Mount Pinatubo, Philippines, and Bingham Canyon,  
264 Utah, USA: *Mineralium Deposita*, v. 36, p.799-806, doi: 10.1007/s001260100209.

265 Hou, Z.Q., Duan, L.F., Lu, Y.J., Zheng, Y.C., Zhu, D.C., Yang, Z.M., Yang, Z.S., Wang, B.D.,  
266 Pei, Y.R., Zhao, Z.D., McCuaig, T.C., 2015a, Lithospheric architecture of the Lhasa  
267 Terrane and its control on ore deposits in the Himalayan-Tibetan orogeny: *Economic*  
268 *Geology*, v. 110, p. 1541-1575, doi: 10.2113/econgeo.110.6.1541.

269 Hou, Z.Q., Yang, Z.M., Lu, Y.J., Kemp, A.I.S., Zheng, Y.C., Li, Q.Y., Tang, J.X., Yang, Z.S.,  
270 and Duan, L.F., 2015b, A genetic linkage between subduction- and collision-related  
271 porphyry Cu deposits in continental collision zones: *Geology*, v. 43, p. 247–250, doi: 10  
272 .1130/G36362.1.

273 Karamyan, K.A., Tayan, R.N., and Guyumdjyan, O.P., 1974, The main features of intrusion  
274 magmatism Zangezur region of the Armenian SSR: *Izvestia of Academy of Sciences of*  
275 *Armenian SSR, Nauki o Zemle* v.1, p. 54-65, (in Russian)

276 Lackey, J.S., Valley, J.W., and Saleeby, J.B., 2005, Supracrustal input to magmas in the deep  
277 crust of Sierra Nevada batholith: evidence from high- $\delta^{18}\text{O}$  zircon: *Earth and Planetary*  
278 *Science Letters*, v. 235, p. 315-330, doi: 10.1016/j.epsl.2005.04.003.

279 Miller, J.S., Matzel, J.P., Miller, C.F., Burgess, S.D., and Miller, R.B., 2007, Zircon growth and  
280 recycling during the assembly of large, composite arc plutons: *Journal of Volcanology*  
281 *and Geothermal Research*, v. 167, p. 282–299, doi: 10.1016/j.jvolgeores.2007.04.019.

282 Moritz, R., Rezeau, H., Ovtcharova, M., Tayan, R., Melkonyan, R., Hovakimyan, S., Ramazanov  
283 V., Selby, D., Ulianov, A., Chiaradia, M., and Putlitz, B., 2016, Long-lived, stationary  
284 magmatism and pulsed porphyry systems during Tethyan subduction to post-collision  
285 evolution in the southernmost Lesser Caucasus, Armenia and Nakhitchevan: *Gondwana*  
286 *Research*, doi: 10.1016/j.gr.2015.10.009 (in press).

287 Richards, J.P., 2015, Tectonic, magmatic, and metallogenic evolution of the Tethyan orogen:  
288 from subduction to collision: *Ore Geology Reviews*, v. 70, p. 323-345, doi:  
289 10.1016/j.oregeorev.2014.11.009.

290 Rohrlach, B.D., and Loucks, R.R., 2005, Multi-million-year cyclic ramp-up of volatiles in a  
291 lower crustal magma reservoir trapped below the Tampakan copper-gold deposit by  
292 Mio-Pliocene crustal compression in the Southern Philippines, *in* Porter, T.M. ed, *Super*  
293 *porphyry copper and gold deposits – a global perspective*: PGC Publishing, v. 2, p. 369-  
294 407.

295 Scaillet, B., 2010, Economic geology: Volatile destruction: *Nature Geoscience*, v.3, p. 456–457,  
296 doi: 10.1038/ngeo908.

297 Sillitoe, R.H., 2010, Porphyry copper systems: *Economic Geology*, v. 105, p. 3–41, doi:  
298 10.2113/gsecongeo.105.1.3.

299 Simmonds, V. and Moazzen, M., 2015, Re–Os dating of molybdenites from Oligocene Cu–Mo–  
300 Au mineralized veins in the Qarachilar area, Qaradagh batholith (northwest Iran):  
301 implications for understanding Cenozoic mineralization in South Armenia,  
302 Nakhchivan, and Iran. *International Geology Review*, v. 57, p. 290–304, doi:  
303 10.1080/00206814.2014.1003339.

304 Tapster, S., Condon, D.J., Naden, J., Noble, S.R., Petterson, M.G., Roberts, N.M.W., Saunders,  
305 A.D., and Smith, D.J., 2016, Rapid thermal rejuvenation of high-crystallinity magma  
306 linked to porphyry copper deposit formation: evidence from the Koloula porphyry  
307 prospect, Solomon Islands: *Earth and Planetary Science Letters*, doi:  
308 <http://dx.doi.org/10.1016/j.epsl.2016.02.046> (in press)

309 Tayan, R.N., 1998, On central magma-ore controlling zone of the Zangezur ore region:  
310 *Proceedings of the National Academy of Sciences of the Republic of Armenia*, v. 51, p.  
311 20-27, (in Russian with English abstract).

312 Von Quadt, A., Erni, M., Martinek, K., Moll, M., Peytcheva, I., and Heinrich, C.A., 2011, Zircon  
313 crystallization and the lifetimes of ore-forming magmatic-hydrothermal systems:  
314 *Geology*, v. 39, p. 731-734, doi: 10.1130/G31966.1.

315

## 316 **FIGURE CAPTIONS**

317 Figure 1. (A) Geochronology of the Meghri-Ordubad pluton and associated Cu-Mo  
318 mineralizations based on 601 concordant zircon U-Pb ages from thirty samples and nine  
319 molybdenite Re-Os ages. The Middle Eocene subduction-related calc-alkaline magmatism has a  
320 duration of  $5.8 \pm 0.8$  m.y. (green), the Late Eocene – Middle Oligocene shoshonitic suite lasted  
321  $9.7 \pm 0.9$  m.y. (blue), and the Late Oligocene shoshonitic to Early Miocene high-K calc-alkaline

322 adakitic magmas were emplaced within  $5.4 \pm 0.4$  m.y. (red). The calculated mean age associated  
323 with each sample does not include antecryst ages (Miller et al., 2007; Appendice DR1 and Table  
324 DR2). Numbers 1 to 30 refer to the sample locations in Figure 2 and the descriptions in Tables  
325 DR1 and DR2. Asterisks indicate dike samples. (B) Zircon *in situ* hafnium (Table DR4) and  
326 oxygen isotopic data (Table DR5) as a function of age. Hf isotope data are shown as individual  
327 analyses (n=365) and as sample median values while oxygen isotopic data are only shown as  
328 median  $\delta^{18}\text{O}$  values (based on 280 analyses) due to limited inter- and intragrain variability.

329

330 Figure 2. Construction of the Meghri-Ordubad pluton based on U-Pb geochronology. Stars  
331 indicate locations of porphyry Cu-Mo deposits for each intrusive stage. Numbers 1 to 30 refer to  
332 dated samples described in Figure 1 and Tables DR1 and DR2. The red dotted lines define  
333 international borders. Geological map modified after Karamyan et al. (1974).

334

335 <sup>1</sup>GSA Data Repository item 2016xxx, Appendice DR1, Figures DR1-DR3, and Tables DR1-  
336 DR5, is available online at [www.geosociety.org/pubs/ft2016.htm](http://www.geosociety.org/pubs/ft2016.htm), or on request from  
337 [editing@geosociety.org](mailto:editing@geosociety.org) or Documents Secretary, GSA, P.O. Box 9140, Boulder, CO 80301,  
338 USA.

Magmatism:

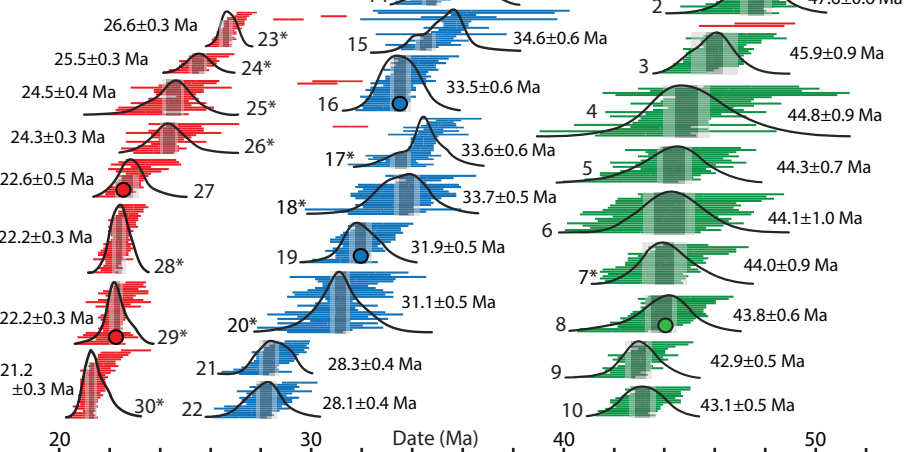
LA-TCP-MS U-Pb zircon

○ ID-TIMS U-Pb zircon

~ Probability density distribution

Cu-Mo mineralization:

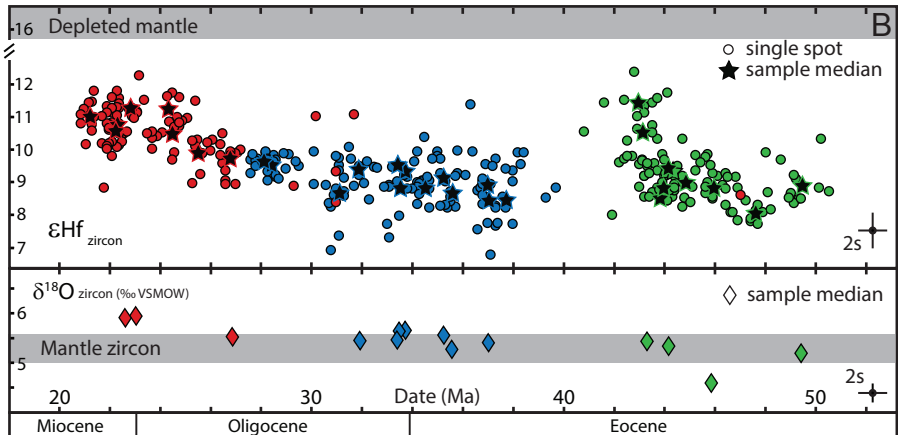
● ID-N-TIMS Re-Os molybdenite



● Cu-rich veins  
20.5±0.1 Ma

● giant PCD  
26.4±0.1 - 27.3±0.1 Ma

● small PCDs  
42.6±0.2 - 44.2±0.2 Ma



B

○ single spot  
★ sample median

◇ sample median

2s

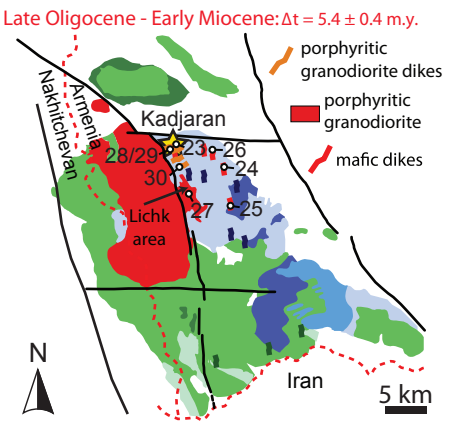
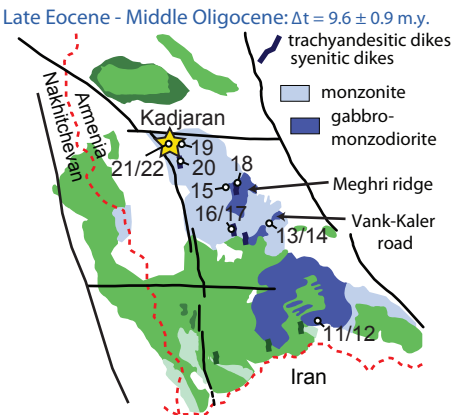
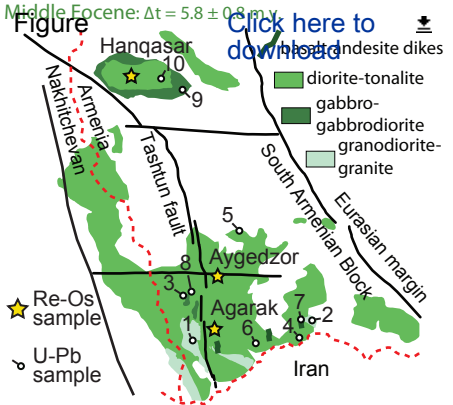
Miocene

Oligocene

Eocene

2s





# 1 Analytical methods

## 2 Major elements whole-rock geochemistry

3 The thirty igneous rock samples from the Meghri–Ordubad pluton selected for dating were analysed for  
4 whole rock geochemistry. The samples were crushed using a steel jaw crusher and subsequently a  
5 hydraulic press and finally powdered to  $<70\ \mu\text{m}$  using a mortar agate mill. Major elements were  
6 analysed on fused lithium tetraborate ( $\text{Li}_2\text{B}_4\text{O}_7$ ) glass beads by X-ray fluorescence (XRF) using a  
7 Philips PW 2400 spectrometer at the University of Lausanne, Switzerland. The  $2\sigma$  uncertainties are  
8  $<1\%$ , except for MgO and  $\text{K}_2\text{O}$   $<3\%$ , based on repeated measurements of the BHVO-1, NIM-N and  
9 NIM-G standards.

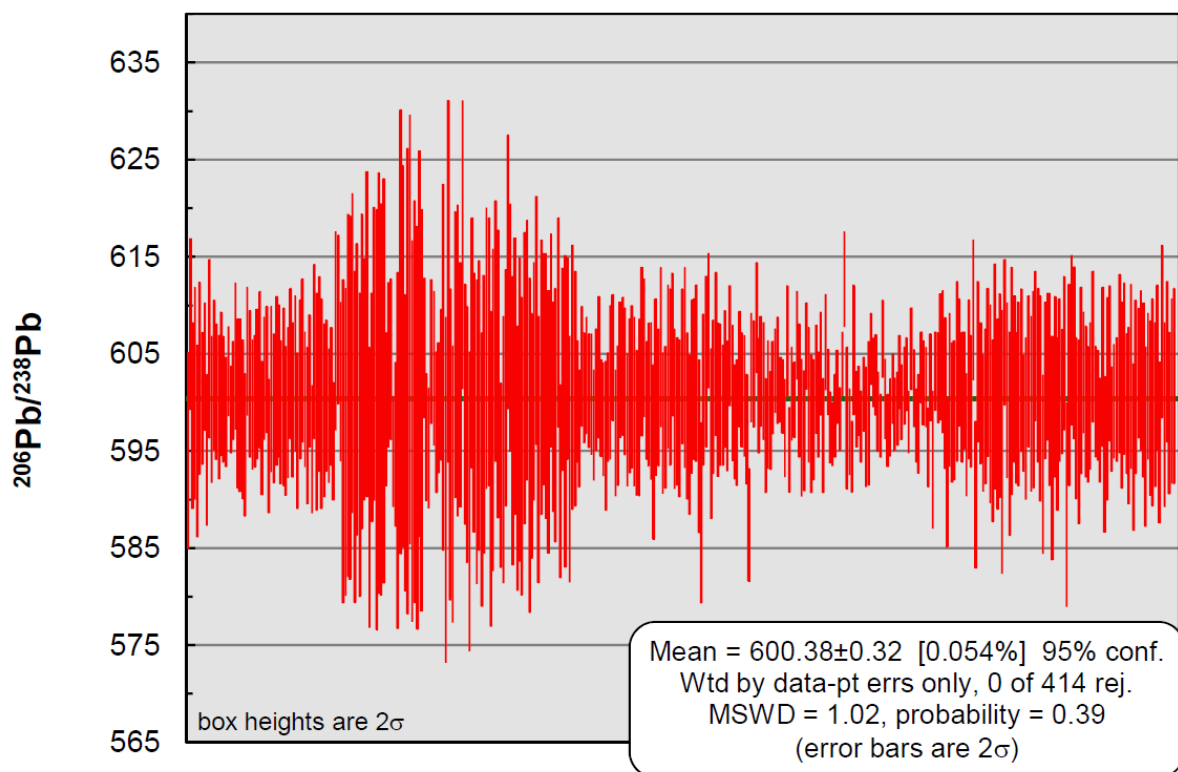
10

## 11 In situ U-Pb zircon dating by LA-ICP-MS

12 The thirty igneous rock samples selected for dating were initially crushed, milled to  $<0.3\ \text{mm}$  and  
13 processed using a gravity separation Wilfley table, a Frantz magnetic separator and a density separation  
14 in diiodomethane liquid at  $3,32\ \text{g}\cdot\text{mL}^{-1}$ . Zircon grains were handpicked under a binocular microscope,  
15 and subsequently mounted in epoxy and polished. Zircon grains textures were revealed by  
16 cathodoluminescence images using a scanning electron microscope JEOL JSM7001F and CamScan  
17 MV2300 at the Institute of Earth Sciences of the University of Geneva and Lausanne, respectively.

18 *In-situ* U-Pb dating of zircon by laser ablation inductively coupled plasma mass spectrometry (LA-ICP-  
19 MS) was carried out using an UP-193FX excimer laser ablation system interfaced to an ELEMENT XR  
20 sector field, single-collector ICP mass spectrometer at the Institute of Earth Sciences of the University  
21 of Lausanne. The operating conditions of the ablation system included a spot size of  $35\ \mu\text{m}$ , a repetition  
22 rate of 5 Hz, and an on-sample energy density of  $\sim 3\ \text{J}/\text{cm}^2$  per pulse. The measurement protocol and  
23 details related to the mass spectrometer optimisation are outlined in Ulianov et al. (2012). A GJ-1  
24 standard zircon with an ID-TIMS  $^{206}\text{Pb}/^{238}\text{U}$  age of  $600.5\pm 0.4\ \text{Ma}$  (Schaltegger et al., *unpublished*; in  
25 Boekhout et al., 2012) was used for the standardisation of the relative sensitivity factor. For the  
26 accuracy control, the Plešovice standard was employed (Sláma et al., 2008). Raw intensity vs. time data

27 were reduced in LAMTRACE (Jackson, 2008). Only homogeneous time resolved  $^{206}\text{Pb}/^{238}\text{U}$  and  
28  $^{207}\text{Pb}/^{235}\text{U}$  spectra corresponding to one single isotope abundance ratio per ablation are reported in this  
29 study. Weighted mean ages and concordia diagrams were obtained using Isoplot (Ludwig, 2008).  
30 The mean age (i.e. crystallization age) is calculated from all concordant zircon population. Based on the  
31 probability density estimate curve and the mean square weighted deviation (MSWD), some samples  
32 exhibit subpopulations (see Figure 1, samples n°1, 13, 14, 15, 17, 21, 23, 27, 28 and 30; Table DR2),  
33 and we only considered the younger subpopulation to represent the crystallization age, the older  
34 subpopulation interpreted as antecrystic or inherited zircons for adjacent rocks (Miller et al., 2007).  
35 Reported errors (2 SD) in Figure 1 are named “internal” and “external” errors. The “internal” error  
36 corresponds to the analytical uncertainties from the sample measurement, while the “external” error  
37 includes the propagation of analytical uncertainties from the sample measurement and the  
38 reproducibility of the measurements on the primary standard GJ-1 (Fig. 1).  
39



40

41 Figure 1: Reproducibility of the GJ1 standard including all analytical sessions carried out over 18 months.

42

### 43 **Re-Os isotopes in molybdenite**

44 Samples for Re-Os dating in molybdenite were selected from various Cu-Mo porphyry deposits  
45 throughout the Meghri-Ordubad pluton (see Figs. 1 and 2; Table DR3). Sample R0280-2\_N2  
46 corresponds to a stockwork-like veinlet mainly filled by quartz-chalcopyrite-molybdenite from  
47 Agarak deposit, whereas samples R0812-3\_Ankaser\_N72p and R0812-7\_Aigedzor\_NRM-0560  
48 were selected from quartz-molybdenite stockwork-like veinlets from Hanqasar and Aygedzor,  
49 respectively. Six samples from quartz-molybdenite (R0280-1\_NI) and quartz-chalcopyrite-  
50 molybdenite (R0758-5\_KJ1509, R0596-2\_KJ-13-25A, R0612-10\_KJ-13-25A, R0391-2\_KJ-10-13A,  
51 and R0758-6\_KJ15X1) stockwork-like veinlets were collected from the giant Kadjaran Cu-Mo  
52 deposit (see Figs. 1 and 2; Table DR3). Grain size of molybdenite varies from 500 $\mu$ m to 2 mm.

53 Analyses were performed in the Laboratory for Sulfide and Source Rock Geochronology and  
54 Geochemistry in the Durham Geochemistry Center at the University of Durham (UK). The  
55 complete analytical procedure for Re-Os determinations is described in Selby and Creaser (2004)  
56 and Selby et al. (2007), and it is briefly described below. Molybdenite samples were dissolved and  
57 equilibrated with a known amount of  $^{185}\text{Re}$  and isotopically normal Os in inverse *aqua-regia* (2:1  
58 16 N  $\text{HNO}_3$  and 12 N  $\text{HCl}$ , 3 mL) at 240°C for 24 h in a Carius tube. Rhenium and Os were isolated  
59 and purified by solvent extraction, microdistillation, and anion exchange chromatography, and  
60 analyzed by negative thermal ionization mass spectrometry (N-TIMS) on a Fisher Scientific  
61 TRITON mass spectrometer using Faraday collectors. Total procedural blanks for Re and Os, are  
62  $2.2 \pm 0.5$  pg and  $0.1 \pm 0.03$  pg, respectively, with an  $^{187}\text{Os}/^{188}\text{Os}$  blank composition of  $0.24 \pm 0.05$   
63 ( $n = 3$ ). Rhenium and Os concentrations and Re-Os molybdenite date uncertainties are presented  
64 at the  $2\sigma$  level, which includes the uncertainties in Re and Os mass spectrometer measurement,  
65 spike and standard Re and Os isotope compositions, and calibration uncertainties of  $^{185}\text{Re}$  and  
66  $^{187}\text{Os}$ . Because a mixed  $^{185}\text{Re}$  and Os tracer solution is used, uncertainties in weights of sample and  
67 tracer solution do not affect the calculated age, and are not considered. However, sample and

68 tracer solution weight uncertainties are considered in determining the uncertainty in the Re and  
69  $^{187}\text{Os}$  concentrations. Uncertainty with and without the  $^{187}\text{Re}$  decay constant (Smoliar et al., 1996;  
70 Selby et al., 2007) is also considered (Table 4).

71

## 72 **In situ zircon Hf isotope analyses**

73 *In-situ* Hf isotope analyses were carried out at the University of Geneva on a Teledyne - Photon  
74 Machines “Analyte G2” laser system equipped with a two volume “HelEx-2” ablation cell (d'Abzac et  
75 al. 2014) and coupled to a Thermo « Neptune Plus » MC-ICP-MS. Ablation was performed over 35  $\mu\text{m}$   
76 spots at a fluence of  $\sim 6\text{J}\cdot\text{cm}^{-2}$  and a repetition rate of 5Hz. Ablated particles were carried through a  $\sim 1.5$   
77 m PTFE tubing using a  $\sim 0.6\text{ L}\cdot\text{min}^{-1}$  He gas flow (99.999% purity) and mixed with  $\sim 2.4\text{ mL}\cdot\text{min}^{-1}$   $\text{N}_2$   
78 and  $\sim 1\text{ L}\cdot\text{min}^{-1}$  Ar before entering the plasma torch. Measurements were performed at low mass  
79 resolution ( $\sim 450$ ) over  $120 \times 1\text{s}$  cycles using the following cup configuration:  $^{171}\text{Yb}$  (L4),  $^{173}\text{Yb}$  (L3),  
80  $^{174}(\text{Yb}+\text{Hf})$  (L2),  $^{175}\text{Lu}$  (L1),  $^{176}(\text{Hf}+\text{Yb}+\text{Lu})$  (C),  $^{177}\text{Hf}$  (H1),  $^{178}(\text{Hf}+\text{Ta})$  (H2),  $^{179}\text{Hf}$  (H3),  $^{181}\text{Ta}$  (H4).  
81 Blanks were acquired following the same method as samples, without ablation, every ca. 10 analyses.  
82 Reference zircons Plešovice (Sláma et al., 2008) and Temora-2 (Woodhead and Hergt, 2005) were  
83 measured after every 5 to 8 unknowns. Plešovice and Temora-2 zircons reach respective  
84  $0.282479 \pm 0.000027$  (n=89) and  $0.282670 \pm 0.000036$  (n=98) over 10 months and 6 measurements  
85 sessions (see details in Table DR 3). These values show a slight offset from the reference values to  
86 which the sample data are normalized. Instrument tuning is then performed so that this offset is (i) as  
87 small as possible ( $< 1\text{ }\epsilon\text{Hf}$ ) and (ii) similar within uncertainty for all the different reference materials  
88 used. This insures that the correction is accurately made for various trace elements concentrations  
89 potentially generating oxide species in the ICP torch and for different amounts of  $^{176}\text{Yb}$  that need to be  
90 corrected (see below).

91 Data reduction was conducted after acquisition by proceeding to a blank subtraction, removing the  
92 isobaric interference of  $^{176}\text{Lu}$  and  $^{176}\text{Yb}$  on mass 176 (e.g. Fisher et al., 2011) and correcting the

93 resulting  $^{176}\text{Hf}/^{177}\text{Hf}$  ratio for mass bias using an exponential law (Albarede et al., 2004). The mass bias  
94 coefficients  $\beta_{\text{Yb}}$  and  $\beta_{\text{Hf}}$  were calculated from the measured  $^{173}\text{Yb}/^{171}\text{Yb}$  and  $^{179}\text{Hf}/^{177}\text{Hf}$  with the  
95 reference values  $^{173}\text{Yb}/^{171}\text{Yb}=1.1234$  (Thirlwall and Anczkiewicz, 2004) and  $^{179}\text{Hf}/^{177}\text{Hf}=0.7325$   
96 (Patchett and Tatsumoto, 1981) respectively. We used  $\beta_{\text{Yb}}$  to correct for Lu mass bias (Yuan et al.,  
97 2008) and the  $^{176}\text{Lu}$  interference was corrected using  $^{176}\text{Lu}/^{175}\text{Lu}=0.02645$  (Thirlwall and Anczkiewicz,  
98 2004). The isobaric interference of  $^{176}\text{Yb}$  is potentially high in zircons and was evaluated using  
99  $^{176}\text{Yb}/^{173}\text{Yb}=0.786954$  (Thirlwall and Anczkiewicz, 2004). Correction for  $^{176}\text{Hf}$  in-growth due to  $^{176}\text{Lu}$   
100  $\beta$ -decay has been calculated (Iizuka and Hirata, 2005) using  $\lambda^{176}\text{Lu}=1.87\times 10^{-11}$  year $^{-1}$  (Söderlund et  
101 al., 2004) and the age determined in this study by U-Pb dating on zircon. The data are expressed as  $\epsilon_{\text{Hf}}$   
102 units following:

$$103 \quad \epsilon_{\text{Hf}} = \left[ \left( \frac{^{176}\text{Hf}}{^{177}\text{Hf}} \right)_{\text{measured}} / \left( \frac{^{176}\text{Hf}}{^{177}\text{Hf}} \right)_{\text{CHUR}} - 1 \right] \times 10000$$

104 with the reference “CHUR” value of 0.282785 is taken from Bouvier et al. (2008).

105

## 106 **In situ zircon O isotope analyses**

107 Oxygen isotopes measurements were carried out on a different zircon sample set than those used for  
108 LA-ICPMS U-Pb zircon dating but their cathodoluminescence patterns are very consistent from one  
109 zircon sample set to another from the same crushed sample. The U-Pb weighted mean dates are  
110 considered to be representative enough to accurately trace the source evolution over 30 Ma (Table  
111 DR2).

112 Sample preparation and secondary ion mass spectrometry (SIMS) were carried out at the Canadian  
113 Centre for Isotopic Microanalysis (CCIM) at the University of Alberta. Polished zircon mid-sections of  
114 unknowns and zircon reference materials were exposed within a 25 mm diameter epoxy mount (M1323)  
115 using diamond grits. The mount was cleaned with a lab soap solution, and de-ionized H<sub>2</sub>O. Prior to  
116 scanning electron microscopy (SEM), the mount was coated with 5 nm of high-purity Au. SEM  
117 characterization was carried out with a Zeiss EVO MA15 instrument equipped with a high-sensitivity,

118 broadband cathodoluminescence (CL) detector. Beam conditions were 15kV and 2 nA sample current.  
119 A further 25 nm of Au was subsequently deposited on the mount prior to SIMS analysis.

120 Oxygen isotopes ( $^{18}\text{O}$ ,  $^{16}\text{O}$ ) in zircon were analyzed using a Cameca IMS 1280 multicollector ion  
121 microprobe. A  $^{133}\text{Cs}^+$  primary beam was operated with impact energy of 20 keV and beam current of ~  
122 2.5 nA. The ~12  $\mu\text{m}$  diameter probe was rastered (18 x 18  $\mu\text{m}$ ) for 75 s prior to acquisition, and then 5  
123 x 5  $\mu\text{m}$  during acquisition, forming rectangular analyzed areas ~15 x 18  $\mu\text{m}$  across and ~2  $\mu\text{m}$  deep.  
124 The normal incidence electron gun was utilized for charge compensation. Negative secondary ions  
125 were extracted through 10 kV into the secondary (Transfer) column. Transfer conditions included a 122  
126  $\mu\text{m}$  entrance slit, a 5 x 5 mm pre-ESA (field) aperture, and 100x sample magnification at the field  
127 aperture, transmitting all regions of the sputtered area. No energy filtering was employed. The  
128 mass/charge separated oxygen ions were detected simultaneously in Faraday cups L'2 ( $^{16}\text{O}^-$ ) and H'2  
129 ( $^{18}\text{O}^-$ ) at mass resolutions ( $m/\Delta m$  at 10%) of 1950 and 2250, respectively. Secondary ion count rates for  
130  $^{16}\text{O}^-$  and  $^{18}\text{O}^-$  were typically  $\sim 2.5 \times 10^9$  and  $5 \times 10^6$  counts/s utilizing  $10^{10} \Omega$  and  $10^{11} \Omega$  amplifier  
131 circuits, respectively. Faraday cup baselines were measured at the start of the analytical session. A  
132 single analysis took 250 s, including pre-analysis rastering, automated secondary ion tuning, and 75 s of  
133 continuous peak counting.

134 Instrumental mass fractionation (IMF) was monitored by repeated analysis of a zircon primary reference  
135 material (RM), S0081 (UAMT1) with  $\delta^{18}\text{O}_{\text{VSMOW}} = +4.87$  (R. Stern, unpublished laser fluorination  
136 data from Ilya Bindeman, University of Oregon) and a secondary zircon RM, S0022 (TEM2) zircon  
137 with  $\delta^{18}\text{O}_{\text{VSMOW}} = +8.2 \text{ ‰}$  (Black et al., 2004). One analysis of the primary and secondary RM was  
138 taken after every 4 and 12 unknowns, respectively. Spot analyses of unknowns totalled 280. The data  
139 set of  $^{18}\text{O}^-/^{16}\text{O}^-$  for S0081 zircon for each of two analytical sessions (N = 45, 51) was processed  
140 collectively for each session, yielding standard deviations of 0.10‰ and 0.07‰, following correction  
141 for systematic within-session drift ( $\leq 0.4 \text{ ‰}$ ). Overall IMF was +1.1 ‰ for both sessions. The  
142 individual spot uncertainties at 95% confidence for  $\delta^{18}\text{O}_{\text{VSMOW}}$  reported include errors relating to within-  
143 spot counting statistics, between-spot (geometric) effects, and correction for instrumental mass

144 fractionation, and average  $\pm 0.19$  ‰. Results for multiple spots on multiple grains of the secondary  
145 RM, S0022, gave session mean values for  $\delta^{18}\text{O}_{\text{VSMOW}} = +8.20 \pm 0.04$  (MSWD = 0.79; N = 18, standard  
146 deviation = 0.08‰) and  $+8.19 \pm 0.05$  (MSWD = 0.56; N = 15, standard deviation = 0.07‰).

147

## 148 **References :**

149 Albarede, F., Telouk, P., Blichert-Toft, J., Boyet, M., Agranier, A., and Nelson, B., 2004, Precise and  
150 accurate isotopic measurements using multiple-collector ICPMS: *Geochimica and Cosmochimica Acta*  
151 v. 68, p. 2725-2744, doi:10.1016/j.gca.2003.11.024.

152 Black, L. P., Kamo, S. L., Allen, C. M., Davis, D., Aleinikoff, J. N., Valley, J. W., Mundil, R.,  
153 Campbell, I. H., Korsch, R. J., Williams, I. S., and Foudoulis, C., 2004, Improved  $^{206}\text{Pb}/^{238}\text{U}$  microprobe  
154 geochronology by the monitoring of a trace-element-related matrix effect; SHRIMP, ID-TIMS, ELA-  
155 ICP-MS and oxygen isotope documentation for a series of zircon standards: *Chemical Geology*, v. 205,  
156 p. 115-140, doi:10.1016/j.chemgeo.2004.01.003.

157 Boekhout F., Spikings R., Sempere T., Chiaradia M., Ulianov A. and Schaltegger U., 2012, Mesozoic  
158 arc magmatism along the southern Peruvian margin during Gondwana breakup and dispersal: *Lithos*, v.  
159 146, p. 48-64, doi:10.1016/j.lithos.2012.04.015.

160 Bouvier, A., Vervoort, J. D., and Patchett, P. J., 2008, The Lu–Hf and Sm–Nd isotopic composition of  
161 CHUR: Constraints from unequilibrated chondrites and implications for the bulk composition of  
162 terrestrial planets: *Earth and Planetary Science Letters*, v. 273, p. 48-57, doi:10.1016/j.epsl.2008.06.010.

163 d'Abzac, F.-X., Czaja, A. D., Beard, B. L., Schauer, J. J., and Johnson, C. M., 2014, Iron Distribution in  
164 Size-Resolved Aerosols Generated by UV-Femtosecond Laser Ablation: Influence of Cell Geometry  
165 and Implications for In Situ Isotopic Determination by LA-MC-ICP-MS: *Geostandards and*  
166 *Geoanalytical Research*, v.38, p. 293-309, doi:10.1111/j.1751-908X.2014.00281.x.



167 Fisher, C. M., Hanchar, J. M., Samson, S. D., Dhuime, B., Blichert-Toft, J., Vervoort, J. D., and Lam,  
168 R., 2011, Synthetic zircon doped with hafnium and rare earth elements: A reference material for in situ  
169 hafnium isotope analysis: *Chemical Geology*, v.286, p. 32-47, doi:10.1016/j.chemgeo.2011.04.013.

170 Iizuka, T. and Hirata, T., 2005, Improvements of precision and accuracy in in situ Hf isotope  
171 microanalysis of zircon using the laser ablation-MC-ICPMS technique: *Chemical Geology*, v.220, p.  
172 121-137, doi:10.1016/j.chemgeo.2005.03.010.

173 Jackson, S., 2008, LAMTRACE data reduction software for LA-ICP-MS. *Laser ablation ICP-MS in the*  
174 *Earth sciences: Current practices and outstanding issues: Mineralogical Association of Canada, Short*  
175 *Course Series 40*, p. 305-307.

176 Ludwig, K.R., 2008, User's Manual for Isoplot 3.70: A geochronological toolkit for Microsoft Excel:  
177 Berkeley Geochronology Center, Special Publication 4, 77 p.

178 Miller, J.S., Matzel, J.P., Miller, C.F., Burgess, S.D., and Miller, R.B., 2007, Zircon growth and  
179 recycling during the assembly of large, composite arc plutons. *Journal of Volcanology and Geothermal*  
180 *Research*, v. 167, p. 282–299, doi: 10.1016/j.jvolgeores.2007.04.019.

181 Patchett, P. J. and Tatsumoto, M., 1981, A routine high-precision method for Lu-Hf isotope  
182 geochemistry and chronology: *Contributions to Mineralogy and Petrology*, v.75, p. 263-267,  
183 doi:10.1007/BF01166766.

184 Pearce, N.J., Perkins, W.T., Westgate, J.A., Gorton, M.P., Jackson, S.E., Neal, C.R., and Chenery, S.P.,  
185 1997, A compilation of new and published major and trace element data for NIST SRM610 and NIST  
186 SRM612 glass reference materials: *Geostandards, Newsletter* 21, p. 115–144, doi:10.1111/j.1751-  
187 908X.1997.tb00538.x.

188 Selby, D., and Creaser, R.A., 2004, Macroscale NTIMS and microscale LA-MC-ICP-MS Re-Os isotopic  
189 analysis of molybdenite: Testing spatial restrictions for reliable Re-Os age determinations, and  
190 implications for the decoupling of Re and Os within molybdenite: *Geochimica et Cosmochimica*

191 Acta, v. 68, p. 3897–3908, doi:10.1016/j.gca.2004.03.022.

192 Selby, D., Creaser, R.A., Stein, H. J., Markey, R. J., and Hannah, J. L., 2007, Assessment of the  $^{187}\text{Re}$   
193 decay constant accuracy and precision: Cross calibration of the  $^{187}\text{Re}$ - $^{187}\text{Os}$  molybdenite and U-Pb  
194 zircon chronometers: *Geochimica et Cosmochimica Acta*, v. 71, p.1999–2013,  
195 doi:10.1016/j.gca.2007.01.008.

196 Sláma, J., Košler, J., Condon, D. J., Crowley, J. L., Gerdes, A., Hanchar, J. M., Horstwood, M. S. A.,  
197 Morris, G. A., Nasdala, L., Norberg, N., Schaltegger, U., Schoene, B., Tubrett, M. N., and Whitehouse,  
198 M. J., 2008, Plešovice zircon - A new natural reference material for U–Pb and Hf isotopic  
199 microanalysis: *Chemical Geology*, v.249, p. 1-35, doi:10.1016/j.chemgeo.2007.11.005.

200 Smoliar, M.I., Walker, R.J., and Morgan, J.W., 1996, Re-Os isotope constraints on the age of Group  
201 IIA, IIIA, IVA, and IVB iron meteorites: *Science*, v. 271, p. 1099–1102, doi:  
202 10.1126/science.271.5252.1099.

203 Söderlund, U., Patchett, P. J., Vervoort, J. D., and Isachsen, C. E., 2004, The  $^{176}\text{Lu}$  decay constant  
204 determined by Lu–Hf and U–Pb isotope systematics of Precambrian mafic intrusions: *Earth and*  
205 *Planetary Science Letters*, v. 219, p. 311-324, doi:10.1016/S0012-821X(04)00012-3.

206 Thirlwall, M. F. and Anczkiewicz, R., 2004, Multidynamic isotope ratio analysis using MC–ICP–MS  
207 and the causes of secular drift in Hf, Nd and Pb isotope ratios: *International Journal of Mass*  
208 *Spectrometry*, v.235, p.59-81, doi:10.1016/j.ijms.2004.04.002.

209 Ulianov A., Muntener O., Schaltegger U. and Bussy F., 2012, The data treatment dependent variability  
210 of U-Pb zircon ages obtained using mono-collector, sector field, laser ablation ICP-MS: *Journal of*  
211 *Analytical Atomic Spectrometry*, v.27, p. 663-676, doi:10.1039/C2JA10358C.

212 Woodhead, J. D. and Hergt, J. M., 2005, A Preliminary Appraisal of Seven Natural Zircon Reference  
213 Materials for In Situ Hf Isotope Determination: *Geostandards and Geoanalytical Research*, v.29, p. 183-  
214 195, doi:10.1111/j.1751-908X.2005.tb00891.x.

215 Yuan, H. L., Gao, S., Dai, M. N., Zong, C. L., Günther, D., Fontaine, G. H., Liu, X. M., and Diwu, C.,  
216 2008, Simultaneous determinations of U–Pb age, Hf isotopes and trace element compositions of zircon  
217 by excimer laser-ablation quadrupole and multiple-collector ICP-MS: *Chemical Geology*, v.247, p. 100-  
218 118, doi:10.1016/j.chemgeo.2007.10.003.

219

220

221

222

223

Table DR1: Summary of location, classification, major (XRF) and selected trace elements (LA-ICP-MS) geochemistry, weighted mean U-Pb zircon ages, median t<sub>Hf</sub> and t<sub>R180</sub> for 20 representative samples from this study and 6 additional samples from Moritz et al. (2016)

Samples	N° Figs. 1 & 2	Location	Longitude	Latitude	Altitude	Rock type (TAS classification in Fig. DR2)	Whole-rock analysis														Zircons			References				
							SiO <sub>2</sub>	TiO <sub>2</sub>	Al <sub>2</sub> O <sub>3</sub>	Fe <sub>2</sub> O <sub>3</sub>	MnO	MgO	CaO	Na <sub>2</sub> O	K <sub>2</sub> O	P <sub>2</sub> O <sub>5</sub>	LOI	Mg#	Cr	Ni	Sr	Y	Mean Age ± 2SD (Ma)		Mean t <sub>Hf</sub> ± 2SD	Mean t <sub>R180</sub> ± 2SD		
							(wt. %)														(ppm)				(Ma)			
AG100A	1	Agaira area	E46 11.734	N08 53.804	923	Granodiorite/Gneiss	70.26	0.34	16.28	2.52	0.01	0.48	2.38	8.81	0.55	0.00	0.86	0.27	26.69	2.00	332.44	14.70	48.9 ± 0.6	8.7 ± 1.1	5.20 ± 0.19	-	this study	
AG100B	-	Agaira area	E46 11.705	N08 53.734	-	Granite	71.50	0.36	16.51	2.77	0.01	0.91	2.58	8.30	0.72	0.11	0.67	0.30	13.00	h.s.	300.00	17.00	<b>48.99 ± 0.07</b>	-	-	-	Moritz et al. 2016	
MR1501	2	Mokai area	E46 13.852	N08 56.303	772	Tonalite	64.92	0.51	15.75	5.22	0.13	1.92	4.99	3.47	2.08	0.15	0.33	0.42	18.00	3.00	269.00	16.00	47.6 ± 0.8	8.0 ± 0.8	-	-	this study	
AG1401	3	Vainuar area	E46 13.320	N08 57.779	1346	Hornblende Gabbro	46.77	0.90	20.17	16.81	0.17	5.41	11.84	2.27	1.70	0.44	0.65	0.50	10.26	14.10	487.70	25.36	45.9 ± 0.9	8.8 ± 1.0	4.51 ± 0.19	-	this study	
AG1504	4	Apaikashen area	E46 11.524	N08 55.012	749	Diorite/Tonalite	66.61	0.64	16.36	8.63	0.14	2.62	5.85	3.38	2.21	0.16	0.46	0.46	21.72	5.58	407.44	22.81	44.8 ± 0.9	9.3 ± 0.9	-	-	this study	
VK1403	5	Vainuar road	E46 13.036	N08 52.034	1787	Quartz monzonite	65.87	0.60	14.99	4.85	0.09	1.11	3.35	5.22	4.45	0.16	0.57	0.32	15.70	2.07	179.25	37.88	44.3 ± 0.7	9.3 ± 0.9	-	-	this study	
AG1403	6	Apaikashen area	E46 11.524	N08 55.012	749	Diorite	58.34	0.90	13.86	9.96	0.21	4.16	5.63	2.63	2.43	0.21	0.73	0.45	20.41	8.22	297.85	37.18	46.1 ± 1	9.4 ± 0.9	-	-	this study	
AG1507	-	Agaira area	E46 13.274	N08 53.862	-	Granodiorite	69.40	0.28	16.51	2.39	0.09	0.48	3.22	5.12	2.01	0.08	0.38	0.28	10.00	h.s.	635.00	7.70	<b>44.80 ± 0.02</b>	-	-	-	Moritz et al. 2016	
AG1406	7	Agaira area	E46 13.802	N08 56.303	772	Basaltic-andesite/diabase	55.05	0.70	17.07	8.29	0.15	4.68	9.02	3.71	1.24	0.14	0.48	0.53	100.27	22.65	433.90	19.27	44 ± 0.9	8.6 ± 0.9	-	-	this study	
AG1402	8	Vainuar area	E46 13.520	N08 57.779	1346	Diorite	59.65	0.68	16.25	7.03	0.16	2.96	6.70	3.24	1.89	0.18	0.37	0.45	21.82	6.09	405.26	24.60	43.8 ± 0.6	8.5 ± 0.9	5.30 ± 0.19	-	this study	
HQ1402	9	Hogopou area	E46 08.393	N08 13.702	1628	Monzonite	52.16	0.57	21.78	6.76	0.17	2.36	9.24	4.31	1.00	0.27	0.57	0.41	12.11	5.10	1511.22	16.38	42.9 ± 0.5	11.3 ± 1.0	-	-	this study	
HQ1403	10	Hogopou area	E46 07.946	N08 13.861	1600	Tonalite	63.93	0.38	16.37	6.57	0.11	1.74	4.70	3.88	2.93	0.19	0.50	0.44	20.70	11.29	362.26	15.92	43.1 ± 0.5	10.4 ± 1.0	5.42 ± 0.20	-	this study	
AG1308A	11	Schwanitz area	E46 02.584	N08 56.873	849	Monzonite (Tephritite)	47.57	1.06	19.73	6.77	0.23	3.81	8.63	4.09	3.25	0.67	1.61	0.48	47.40	17.22	1907.06	26.94	37.8 ± 0.8	8.4 ± 1.3	5.37 ± 0.19	-	this study	
AG1308B	12	Schwanitz area	E46 02.584	N08 56.873	849	Monzonite	53.52	0.51	22.51	4.26	0.12	1.09	7.17	6.05	3.44	0.32	1.06	0.38	13.94	1.97	2891.89	18.78	37 ± 0.4	8.4 ± 1.3	5.37 ± 0.19	-	this study	
VK1404	13	Near Kalar	E46 16.975	N08 53.411	2267	Monzonite	48.95	0.92	17.85	6.44	0.16	5.20	10.24	3.55	4.49	0.36	0.52	18.84	15.58	1371.15	21.51	35.7 ± 0.8	8.9 ± 1.0	-	-	this study		
VK1405	14	Near Kalar	E46 16.975	N08 53.411	2267	Monzonite	53.03	0.54	21.27	6.08	0.09	2.14	8.27	4.06	2.56	0.67	0.40	0.41	21.33	14.20	1534.87	20.80	34.8 ± 0.5	8.8 ± 1.2	5.28 ± 0.20	-	this study	
MR1403	15	Mighty ridge	E46 14.495	N08 05.877	2762	Monzonite	52.66	0.74	20.00	6.33	0.14	2.64	7.19	4.58	3.80	0.55	0.45	16.17	6.32	1469.97	25.11	34.6 ± 0.6	8.1 ± 1.3	5.68 ± 0.18	-	this study		
L1130A1	16	Vainuar road	E46 15.579	N08 03.469	2000	Monzonite	47.86	0.90	21.53	6.77	0.13	3.43	10.85	3.26	1.62	0.51	0.91	0.44	2.80	3.59	1332.91	22.62	33.5 ± 0.6	8.8 ± 1.0	5.64 ± 0.19	-	this study	
L1130B	17	Vainuar road	E46 15.579	N08 03.468	2000	Syenitic dike	59.80	0.59	18.54	4.73	0.13	1.29	3.38	5.20	5.36	0.31	0.48	0.35	8.20	h.s.	685.43	27.37	33.8 ± 0.6	8.8 ± 1.0	-	-	this study	
MR1402(Kr,Zr)	-	Mighty ridge	E46 13.287	N08 06.159	2685	Hornblende Gabbro	41.69	1.46	19.04	11.89	0.21	6.84	12.89	2.30	0.69	1.23	0.53	0.53	14.06	h.s.	1816.68	34.15	<b>33.49 ± 0.02</b>	9.5 ± 0.6	5.61 ± 0.18	-	this study / Moritz et al. 2016	
KJ1116	18	Mighty ridge	E46 13.287	N08 06.156	2685	Trachyandesite dike	60.26	0.90	17.54	5.95	0.13	1.77	5.09	4.37	3.57	0.40	0.36	0.40	13.90	2.78	1103.98	24.42	33.7 ± 0.5	9.4 ± 0.5	5.62 ± 0.19	-	this study	
KJ100A	19	Atia	E46 12.745	N08 09.076	1662	Monzonite	57.09	0.82	18.62	5.29	0.12	2.02	4.00	4.28	6.05	0.41	0.71	0.43	8.00	5.28	682.00	21.93	31.9 ± 0.5	9.4 ± 0.8	-	-	this study	
KJ100B	-	Atia	E46 09.028	N08 09.084	-	Monzonite	56.96	0.80	17.89	6.50	0.13	2.69	4.97	3.85	4.60	0.30	0.50	0.45	11.89	8.31	722.00	25.80	<b>31.80 ± 0.02</b>	-	5.47 ± 0.19	-	Moritz et al. 2016	
KJ1308	20	Road to Mgnyi	E46 11.534	N08 08.656	1220	Syenitic dike	60.88	0.90	18.87	4.24	0.09	0.99	2.00	5.57	7.88	0.17	0.50	0.32	2.50	h.s.	512.01	19.69	31.1 ± 0.5	8.7 ± 1.0	-	-	this study	
KJ1308	21	Kajapan open pit	E46 08.020	N08 08.972	1866	Gabbro (weakly altered)	47.48	0.97	18.27	10.28	0.15	5.57	10.45	2.90	1.02	0.56	1.09	0.53	54.00	37.00	1369.70	18.30	28.3 ± 0.4	9.5 ± 0.6	-	-	this study	
KJ1309	22	Kajapan open pit	E46 08.020	N08 08.972	1866	Monzonite (heavily altered)	-	-	-	-	-	-	-	-	-	-	-	-	-	-	-	-	-	-	-	-	-	this study
KJ1302A	23	Kajapan Open pit	E46 08.474	N08 08.757	1867	Trachyandesite dike	58.41	0.84	14.20	4.70	0.12	1.72	4.30	6.23	6.70	0.44	0.48	0.42	74.50	39.96	225.79	10.48	36.5 ± 0.3	9.7 ± 0.9	5.54 ± 0.19	-	this study	
KJ1302B	24	Near Kamen	E46 15.020	N08 07.515	2143	Trachybasalt dike	46.90	1.06	13.68	7.52	0.14	3.13	6.56	2.84	2.49	0.56	0.76	0.55	397.90	145.86	2370.00	16.79	25.5 ± 0.9	9.9 ± 1.1	-	-	this study	
MR1401	25	Mighty Ridge	E46 12.808	N08 06.430	2547	Trachyandesite dike	61.43	0.80	15.40	4.47	0.08	2.29	4.11	5.68	3.85	0.27	0.50	0.50	44.51	19.02	801.97	13.21	24.5 ± 0.4	11.2 ± 0.9	-	-	this study	
KJ1307	26	Road to Puhua	E46 12.907	N08 08.162	1860	Trachybasalt dike	50.95	0.78	14.13	6.72	0.11	7.82	7.18	3.17	2.01	0.37	0.59	0.70	279.70	200.54	739.34	14.68	24.3 ± 0.3	10.4 ± 0.8	-	-	this study	
L11301	27	Loka area	E46 10.368	N08 01.781	1707	Porphyrlic Granodiorite	66.66	0.47	14.95	3.27	0.05	2.02	3.21	4.01	3.72	0.22	0.61	0.55	68.86	33.30	616.28	9.51	23.8 ± 0.5	11.2 ± 1.2	5.97 ± 0.19	-	this study	
L11303	-	Loka area	E46 10.375	N08 02.777	-	Porphyrlic Granodiorite	66.97	0.49	15.28	3.35	0.05	2.08	3.19	3.88	3.00	0.21	0.6	0.55	58.00	39.00	670.00	10.00	<b>22.46 ± 0.02</b>	-	-	-	Moritz et al. 2016	
KJ1305A	28	Kajapan Open pit	E46 08.474	N08 08.644	1901	porphyritic granodiorite dike	61.25	0.42	14.35	3.24	0.06	2.00	4.23	1.46	4.02	0.30	0.6	0.56	85.90	26.39	404.98	9.44	22.2 ± 0.3	10.7 ± 0.8	-	-	this study	
KJ1305B	29	Kajapan Open pit	E46 08.028	N08 08.972	1866	porphyritic granodiorite dike	62.85	0.44	15.19	3.62	0.06	1.89	2.85	1.36	3.59	0.23	0.5	0.48	31.60	23.97	433.59	10.16	22.2 ± 0.3	10.5 ± 1.0	5.92 ± 0.19	-	this study	
KJ1311A	-	Kajapan Open pit	E46 08.316	N08 08.616	-	Basalt-andesite dike	54.26	0.54	15.98	3.92	0.11	2.82	5.98	0.17	4.80	0.26	11.68	0.59	60.00	28.00	274.00	11.00	<b>22.20 ± 0.01</b>	-	-	-	Moritz et al. 2016	
KJ1311B	30	Road to Mgnyi	E46 11.054	N08 08.547	1952	Trachyandesite dike	64.42	0.64	14.94	4.64	0.10	4.47	6.24	9.57	3.49	0.37	0.56	0.39	91.70	44.00	719.68	12.75	21.2 ± 0.3	10.9 ± 0.8	-	-	this study	

Red numbers correspond to trace elements measured by XRF

Red dots refer to Ca-ED-TIMS ages from Moritz et al. (2016)

Table DR2: Results of in situ LA-ICP-MS U-Pb dating. Shaded area indicates the errors used to calculate the weighted mean age.

Analysis (event)	Age (Ma)	$^{206}\text{Pb}/^{238}\text{U}$	$^{207}\text{Pb}/^{235}\text{U}$	$^{206}\text{Pb}/^{238}\text{U}$	$^{207}\text{Pb}/^{235}\text{U}$	$^{206}\text{Pb}/^{238}\text{U}$	$^{207}\text{Pb}/^{235}\text{U}$	$^{206}\text{Pb}/^{238}\text{U}$	$^{207}\text{Pb}/^{235}\text{U}$	Corr. Corr.	Comment
Mean ± 1σ	10.4	0.000	0.000	0.000	0.000	0.000	0.000	0.000	0.000		
1σ											
2σ											
3σ											
4σ											
5σ											
6σ											
7σ											
8σ											
9σ											
10σ											
11σ											
12σ											
13σ											
14σ											
15σ											
16σ											
17σ											
18σ											
19σ											
20σ											
21σ											
22σ											
23σ											
24σ											
25σ											
26σ											
27σ											
28σ											
29σ											
30σ											
31σ											
32σ											
33σ											
34σ											
35σ											
36σ											
37σ											
38σ											
39σ											
40σ											
41σ											
42σ											
43σ											
44σ											
45σ											
46σ											
47σ											
48σ											
49σ											
50σ											
51σ											
52σ											
53σ											
54σ											
55σ											
56σ											
57σ											
58σ											
59σ											
60σ											
61σ											
62σ											
63σ											
64σ											
65σ											
66σ											
67σ											
68σ											
69σ											
70σ											
71σ											
72σ											
73σ											
74σ											
75σ											
76σ											
77σ											
78σ											
79σ											
80σ											
81σ											
82σ											
83σ											
84σ											
85σ											
86σ											
87σ											
88σ											
89σ											
90σ											
91σ											
92σ											
93σ											
94σ											
95σ											
96σ											
97σ											
98σ											
99σ											
100σ											

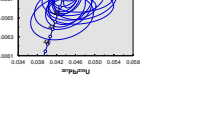
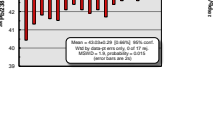
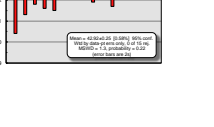
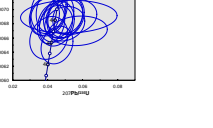
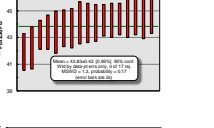
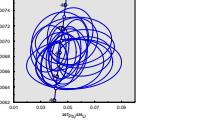
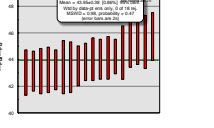
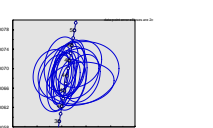
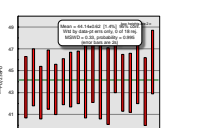
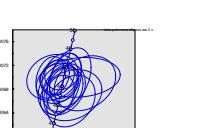
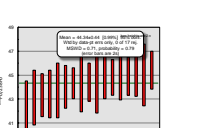
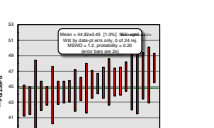
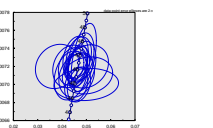
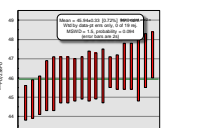
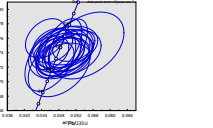
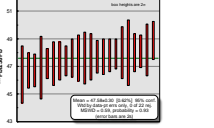
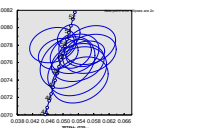
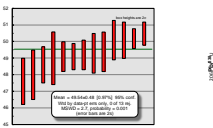
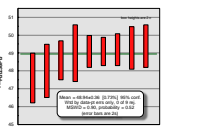










Table DR3: Re-Os data for molybdenite from various PCDs hosted by the Meghri-Ordubad pluton

Sample	Location	wt (g)	Re (ppm)	±	<sup>187</sup> Re (ppm)	±	<sup>187</sup> Os (ppb)	±	Age (Ma)	± <sup>a</sup>	± <sup>b</sup>	Description
RO280-2_N2 <sup>d</sup>	Agarak	0.024	538.8	1.9	338.7	1.2	249.6	0.7	44.23	0.18	0.22	stockwork-like veins (quartz-molybdenite-chalcopyrite)
RO812-3_Ankaser_N72p <sup>d</sup>	Hanqasar	0.022	76.3	0.3	47.9	0.2	34.5	0.1	43.14	0.17	0.22	stockwork-like veins (quartz-molybdenite)
RO812-7_Aigedzor_NRM-0560 <sup>d</sup>	Aygedzor	0.011	1141.0	5.5	717.2	3.5	509.5	2.3	42.62	0.17	0.22	stockwork-like veins (quartz-molybdenite)
RO758-5_K11509	Kadjaran	0.020	238.6	0.9	150.0	0.6	68.2	0.2	27.28	0.11	0.14	stockwork-like veins (quartz-molybdenite-chalcopyrite)
RO280-1_N1 <sup>d</sup>	Kadjaran	0.042	368.3	1.2	231.5	0.8	104.9	0.3	27.19	0.11	0.14	stockwork-like veins (quartz-molybdenite)
RO596-2_KJ-13-25A	Kadjaran	0.015	350.8	1.4	220.5	0.9	97.9	0.4	26.65	0.11	0.14	sheared stockwork-like veins (quartz-molybdenite-chalcopyrite)
RO612-10_KJ-13-25A <sup>c</sup>	Kadjaran	0.027	365.4	1.3	229.6	0.8	101.9	0.3	26.64	0.11	0.14	sheared stockwork-like veins (quartz-molybdenite-chalcopyrite)
RO391-2_KJ-10-13A <sup>d</sup>	Kadjaran	0.050	160.4	0.5	100.8	0.3	44.4	0.1	26.43	0.11	0.13	stockwork-like veins (quartz-molybdenite-chalcopyrite)
RO758-6_K115X1	Kadjaran	0.020	360.6	1.3	226.6	0.8	77.4	0.2	20.48	0.08	0.10	reopening of moly stockwork-like veins (quartz-molybdenite-chalcopyrite)

<sup>a</sup> age uncertainty includes all analytical sources of uncertainty

<sup>b</sup> age uncertainty includes all analytical sources of uncertainty and the uncertainty in the <sup>187</sup>Re decay constant

<sup>c</sup> repeat analysis. Aliquot analyzed comes from one mineral separate.

<sup>d</sup> Re-Os ages cited in Moritz et al. (2016)

Table DR4: Results of in situ MC-ICP-MS cHf isotope analyses.

Analysis (n=65)	# cycles integrate d	SAMPLES										U-Pb Age [Ma]	176Hf/177Hf (t) CHUR <sup>a</sup>	176Hf/177Hf (t)	εHf (t)	2σe	
		176Hf/177Hf	176Hf/177Hf std corrected	176Lu/177Hf	2σe	173Yb/177Hf	1σe	174Hf/177Hf	2σe	178Hf/177Hf	2σe						
<b>AG1304A (s080515) n=11</b>																	
AG1304A_1.dat	80	0.283003	0.283000	1.88E-05	0.003034	0.03E-04	0.148993	9.62E-03	0.008679	2.36E-05	1.487268	0.000126001	50.5	0.282753	0.282997	8.6	1.3
AG1304A_2.dat	80	0.282996	0.282993	1.47E-05	0.001209	4.18E-05	0.056661	1.93E-03	0.008656	1.36E-05	1.487249	0.000116556	49.3	0.282754	0.282991	8.4	1.0
AG1304A_3.dat	100	0.283005	0.283002	2.80E-05	0.006900	7.42E-05	0.417637	0.05E-03	0.008741	3.97E-05	1.487267	0.000111033	50.2	0.282753	0.283043	10.2	2.0
AG1304A_4.dat	70	0.282994	0.282991	1.61E-05	0.003402	1.27E-04	0.159420	4.11E-03	0.008686	2.06E-05	1.487285	0.000142396	49.1	0.282754	0.282988	8.3	1.1
AG1304A_5.dat	60	0.283001	0.282997	1.79E-05	0.005922	1.12E-05	0.041956	9.24E-04	0.008665	1.20E-05	1.487278	0.000147851	49	0.282754	0.282987	8.6	1.2
AG1304A_6.dat	80	0.283037	0.283034	2.41E-05	0.001793	3.04E-05	0.072572	1.92E-03	0.008675	2.46E-05	1.487265	0.000219872	48	0.282755	0.283032	9.8	1.7
AG1304A_7.dat	90	0.282996	0.282992	1.48E-05	0.001019	2.58E-05	0.043738	2.83E-04	0.008687	1.13E-05	1.487227	0.000122337	49.4	0.282754	0.282991	8.4	1.0
AG1304A_8.dat	120	0.283014	0.283010	1.15E-05	0.001317	3.55E-05	0.053413	4.81E-04	0.008666	1.09E-05	1.487277	0.000146025	49.2	0.282754	0.283009	9.0	0.8
AG1304A_9.dat	100	0.283030	0.283026	1.60E-05	0.002071	7.36E-06	0.042508	7.74E-04	0.008672	1.10E-05	1.487245	0.000119325	48.8	0.282754	0.283025	9.6	1.1
AG1304A_11.dat	70	0.283016	0.283013	1.39E-05	0.001040	1.42E-05	0.043985	9.39E-04	0.008658	1.23E-05	1.487229	0.000127835	49.1	0.282754	0.283012	9.1	1.0
AG1304A_12.dat	80	0.283005	0.283002	1.46E-05	0.001327	4.72E-05	0.056823	9.52E-04	0.008655	1.23E-05	1.487268	0.000129036	50.1	0.282754	0.283000	8.7	1.0
Median ± 2SD																8.7	1.3
<b>MA1501 (s07-081015) n=13</b>																	
MA1501_01	110	0.282958	0.282974	9.84E-06	0.001256	5.18E-05	0.048253	1.04E-03	0.008658	7.28E-06	1.487266	0.000108828	47.4	0.282755	0.282973	7.7	0.7
MA1501_02	120	0.282967	0.282983	8.60E-06	0.001364	7.51E-05	0.056342	1.86E-03	0.008675	7.13E-06	1.487258	7.82789E-05	47.6	0.282755	0.282982	8.0	0.6
MA1501_03	120	0.282967	0.282983	7.48E-06	0.001352	2.34E-05	0.053815	7.77E-04	0.008659	7.07E-06	1.487255	8.08356E-05	46.7	0.282756	0.282981	8.0	0.5
MA1501_04	80	0.282973	0.282988	1.10E-05	0.001508	2.46E-05	0.060278	6.83E-04	0.008666	8.44E-06	1.487238	9.20218E-05	47.7	0.282755	0.282987	8.2	0.8
MA1501_05	100	0.282974	0.282989	9.60E-06	0.001598	1.89E-05	0.062849	6.63E-04	0.008665	7.75E-06	1.487253	0.000101268	46.4	0.282756	0.282988	8.2	0.7
MA1501_06	120	0.282953	0.282959	8.93E-06	0.001151	1.16E-05	0.045898	3.81E-04	0.008657	6.07E-06	1.487247	8.13876E-05	48.1	0.282755	0.282988	8.6	0.8
MA1501_07	120	0.282968	0.282982	8.11E-06	0.001537	6.91E-05	0.058773	1.29E-03	0.008661	7.86E-06	1.487282	6.80148E-05	47.9	0.282755	0.282981	8.0	0.8
MA1501_08	120	0.282978	0.282994	7.48E-06	0.001591	4.80E-05	0.062274	6.66E-04	0.008657	7.07E-06	1.487246	7.60765E-05	48.9	0.282754	0.282982	8.4	0.5
MA1501_09	120	0.282968	0.282984	8.28E-06	0.001387	6.05E-05	0.052438	9.61E-04	0.008660	6.31E-06	1.487247	9.8911E-05	47.6	0.282755	0.282983	8.1	0.8
MA1501_10	120	0.282961	0.282977	8.27E-06	0.001603	6.01E-05	0.060294	1.15E-03	0.008668	7.59E-06	1.487280	7.23919E-05	47.4	0.282755	0.282975	7.7	0.8
MA1501_11	120	0.282977	0.282992	7.72E-06	0.001417	2.11E-05	0.053355	3.79E-04	0.008674	6.72E-06	1.487242	7.73709E-05	47.2	0.282755	0.282991	8.3	0.5
MA1501_12	120	0.282959	0.282975	7.77E-06	0.001445	4.59E-05	0.056207	8.00E-04	0.008651	6.86E-06	1.487251	8.18464E-05	46.9	0.282756	0.282974	7.7	0.6
MA1501_13	120	0.282956	0.282971	6.14E-06	0.001530	4.89E-05	0.058721	1.97E-03	0.008652	7.00E-06	1.487258	7.79846E-05	47.2	0.282755	0.282970	7.6	0.7
Median ± 2SD																8.0	0.6
<b>AG1401 (s080515) n=10</b>																	
AG1401_1.dat	80	0.283019	0.283015	1.50E-05	0.003241	1.04E-04	0.138299	2.55E-03	0.008677	2.21E-05	1.487263	0.000102319	46.8	0.282756	0.283012	9.1	1.1
AG1401_2.dat	110	0.283007	0.283004	1.41E-05	0.001694	2.49E-05	0.063874	5.54E-04	0.008665	1.31E-05	1.487314	9.78011E-05	46.9	0.282756	0.283002	8.7	1.0
AG1401_3.dat	110	0.283019	0.283016	1.42E-05	0.002534	8.95E-05	0.097771	1.29E-03	0.008675	1.54E-05	1.487284	0.000102142	46.1	0.282756	0.283013	9.1	1.0
AG1401_4.dat	110	0.282987	0.282984	1.44E-05	0.002684	1.17E-04	0.106953	3.11E-03	0.008670	1.48E-05	1.487292	0.000104865	46.6	0.282756	0.282981	8.0	1.0
AG1401_5.dat	110	0.283038	0.283034	1.33E-05	0.002521	1.12E-04	0.074522	4.17E-03	0.008668	1.73E-05	1.487278	0.000107787	45.7	0.282756	0.283032	9.8	0.9
AG1401_6.dat	110	0.282998	0.282995	1.41E-05	0.001853	1.46E-05	0.078193	1.95E-03	0.008664	1.42E-05	1.487297	0.000112507	45.9	0.282756	0.282993	8.4	1.0
AG1401_7.dat	80	0.283000	0.282996	1.46E-05	0.001565	4.65E-05	0.064369	1.95E-03	0.008658	1.30E-05	1.487284	0.000118989	45.9	0.282756	0.282995	8.4	1.0
AG1401_8.dat	110	0.283011	0.283007	1.38E-05	0.002660	1.98E-04	0.112226	4.79E-03	0.008669	1.61E-05	1.487307	0.000104748	46.3	0.282756	0.283005	8.8	1.0
AG1401_9.dat	110	0.283021	0.283018	1.41E-05	0.002409	1.17E-04	0.088988	2.11E-03	0.008674	1.51E-05	1.487286	0.000113874	45.9	0.282756	0.283016	9.2	1.0
AG1401_10.dat	110	0.283004	0.283001	1.49E-05	0.002540	1.85E-04	0.104073	3.67E-03	0.008671	1.39E-05	1.487274	0.00010908	45.6	0.282756	0.282999	8.6	1.1
Median ± 2SD																8.8	1.0
<b>AG1404 (s080515) n=12</b>																	
AG1404_1.dat	120	0.283019	0.283015	1.23E-05	0.001403	4.59E-05	0.066975	1.17E-03	0.008671	1.21E-05	1.487264	9.12844E-05	44.7	0.282757	0.283014	9.1	0.9
AG1404_2.dat	120	0.283012	0.283009	1.29E-05	0.001814	6.09E-05	0.084014	1.67E-03	0.008662	1.50E-05	1.487310	0.000150863	44.4	0.282757	0.283007	8.9	0.9
AG1404_3.dat	120	0.283038	0.283034	1.71E-05	0.001814	4.66E-05	0.081269	1.52E-03	0.008671	1.50E-05	1.487347	0.000107073	43.8	0.282757	0.283003	8.7	1.2
AG1404_4.dat	35	0.283034	0.283031	1.87E-05	0.000916	3.95E-05	0.048791	1.96E-03	0.008693	1.69E-05	1.487425	0.000287254	45.6	0.282756	0.283030	9.7	1.3
AG1404_5.dat	110	0.283019	0.283016	1.29E-05	0.001448	1.99E-05	0.068346	1.32E-03	0.008679	1.18E-05	1.487236	0.000108509	43.2	0.282758	0.283015	9.1	0.9
AG1404_5b.dat	80	0.282991	0.282988	1.28E-05	0.001163	4.05E-05	0.052753	5.13E-04	0.008649	1.06E-05	1.487248	0.000152603	44.7	0.282757	0.282987	8.1	0.9
AG1404_6.dat	120	0.283013	0.283010	1.28E-05	0.001282	1.44E-05	0.057093	1.52E-03	0.008666	1.18E-05	1.487194	0.000108189	43.9	0.282757	0.283009	8.9	0.9
AG1404_7.dat	120	0.283024	0.283021	1.11E-05	0.001303	3.39E-05	0.055919	3.42E-04	0.008678	1.21E-05	1.487240	0.000107691	43.7	0.282758	0.283020	9.3	0.8
AG1404_8.dat	120	0.283008	0.283005	1.23E-05	0.001455	7.66E-05	0.086207	2.67E-03	0.008660	1.13E-05	1.487244	0.000117788	45.6	0.282756	0.283004	8.8	0.9
AG1404_9.dat	60	0.283020	0.283016	1.48E-05	0.001292	3.38E-05	0.062659	1.85E-03	0.008665	1.30E-05	1.487225	0.000153355	46.4	0.282756	0.283015	9.2	1.0
AG1404_10.dat	100	0.283016	0.283013	1.20E-05	0.001160	3.74E-05	0.053469	1.67E-03	0.008656	1.03E-05	1.487218	0.000123388	46.5	0.282756	0.283012	9.1	0.8
AG1404_11.dat	110	0.283006	0.283003	1.29E-05	0.001199	3.13E-05	0.054368	1.68E-03	0.008651	1.01E-05	1.487239	0.000120272	46.4	0.282756	0.283002	8.7	0.8
Median ± 2SD																9.0	0.8
<b>VK1403 (s050215) n=10</b>																	
VK1403_01.dat	120	0.283026	0.283020	1.09E-05	0.001158	4.68E-05	0.048072	1.18E-03	0.008681	8.84E-06	1.487233	0.00010832					

AG1406 (s080515) n=10																	
AG1406_1.dat	120	0.283010	0.283007	1.15E-05	0.001342	2.48E-05	0.006199	1.44E-03	0.008659	1.14E-05	1.487273	0.00011504	43	0.282758	0.283006	8.8	0.8
AG1406_2.dat	120	0.283002	0.283004	1.14E-05	0.001352	2.39E-05	0.006203	1.43E-03	0.008659	1.14E-05	1.487273	0.00011504	43	0.282758	0.283006	8.8	0.8
AG1406_3.dat	120	0.282998	0.282994	1.31E-05	0.001352	2.48E-05	0.006217	1.41E-03	0.008659	1.14E-05	1.487273	0.00011504	43	0.282758	0.283006	8.8	0.8
AG1406_4.dat	120	0.283009	0.283005	1.03E-05	0.001187	3.11E-05	0.005993	1.11E-03	0.008666	1.10E-05	1.487284	0.000110931	45.1	0.282757	0.283004	8.8	0.9
AG1406_5.dat	120	0.283022	0.283019	1.37E-05	0.003034	1.35E-04	0.019088	2.80E-03	0.008672	1.73E-05	1.487281	0.000110727	44.2	0.282757	0.283016	9.2	1.0
AG1406_6.dat	120	0.283034	0.283031	1.31E-05	0.001348	2.95E-05	0.006213	1.39E-03	0.008673	1.39E-05	1.487273	0.000129415	43.1	0.282758	0.283000	8.8	0.9
AG1406_7.dat	70	0.283001	0.282998	1.41E-05	0.001385	1.71E-05	0.006410	1.32E-03	0.008652	1.43E-05	1.487281	0.000128231	43.4	0.282758	0.282997	8.5	1.0
AG1406_8.dat	120	0.283019	0.283016	1.26E-05	0.001536	4.70E-05	0.006323	1.07E-03	0.008659	1.20E-05	1.487280	0.000105959	43.2	0.282758	0.283015	9.1	0.9
AG1406_9.dat	120	0.283012	0.283009	1.23E-05	0.001242	1.29E-05	0.006124	1.29E-03	0.008675	1.29E-05	1.487286	0.000164465	45.7	0.282758	0.283002	8.8	0.9
AG1406_10.dat	120	0.283037	0.283033	1.22E-05	0.001387	1.53E-05	0.006233	1.76E-04	0.008666	1.05E-05	1.487273	0.000121216	45.2	0.282757	0.283002	8.8	0.9
Median ± 2SD																	

AG1402 (s040215) n=10																	
AG1402_10.dat	90	0.282980	0.283001	1.89E-05	0.000848	1.36E-05	0.038209	4.74E-04	0.008682	1.13E-05	1.487247	0.000138207	43.7	0.282758	0.283001	8.6	1.1
AG1402_09.dat	120	0.282972	0.282994	1.43E-05	0.001057	6.04E-05	0.042792	1.13E-03	0.008690	1.40E-05	1.487331	0.000122408	44.1	0.282757	0.282993	8.3	1.0
AG1402_08.dat	120	0.282962	0.282984	1.29E-05	0.001788	1.49E-04	0.017307	2.82E-03	0.008650	1.34E-05	1.487255	0.000119185	41.9	0.282758	0.282982	7.9	0.9
AG1402_07.dat	120	0.282976	0.282997	1.30E-05	0.000528	2.08E-05	0.039453	6.61E-04	0.008669	1.04E-05	1.487303	0.000101999	44.1	0.282757	0.282996	8.5	0.9
AG1402_06.dat	120	0.282988	0.283009	1.34E-05	0.001226	2.57E-05	0.056652	5.21E-04	0.008675	1.19E-05	1.487292	0.000125556	44.7	0.282757	0.283008	8.9	0.9
AG1402_05.dat	120	0.282979	0.283001	1.33E-05	0.002104	2.42E-04	0.089844	6.25E-03	0.008670	1.31E-05	1.487289	0.000110687	44.3	0.282757	0.282999	8.6	0.9
AG1402_04.dat	120	0.282976	0.282997	1.46E-05	0.000974	1.73E-05	0.040007	3.03E-04	0.008659	1.83E-05	1.487307	0.000121234	44.3	0.282757	0.282996	8.5	1.0
AG1402_03.dat	80	0.282977	0.282998	1.49E-05	0.001179	5.50E-05	0.053625	1.39E-03	0.008671	1.56E-05	1.487276	0.000147716	43.2	0.282758	0.282997	8.5	1.1
AG1402_02.dat	120	0.282981	0.283002	1.19E-05	0.000961	1.86E-05	0.038603	3.18E-04	0.008663	1.03E-05	1.487310	0.000115753	44.4	0.282757	0.283002	8.6	0.8
AG1402_01.dat	120	0.282984	0.283005	1.13E-05	0.000984	4.50E-05	0.039133	8.39E-04	0.008680	8.72E-06	1.487272	0.000135555	43.7	0.282758	0.283005	8.7	0.8
Median ± 2SD																	

HQ1402 (s080515) n=9																	
HQ1402_1.dat	120	0.283003	0.283000	1.22E-05	0.000948	4.01E-05	0.040248	1.05E-03	0.008649	1.01E-05	1.487248	0.27827E-05	43.5	0.282758	0.283009	10.7	0.9
HQ1402_2.dat	120	0.282996	0.283003	1.29E-05	0.000971	2.41E-05	0.042303	4.29E-04	0.008670	9.41E-06	1.487280	0.000103868	42.4	0.282758	0.283002	11.4	0.8
HQ1402_3.dat	80	0.283112	0.283108	1.70E-05	0.002616	2.44E-04	0.120061	5.24E-03	0.008711	1.78E-05	1.487324	0.000134517	42.8	0.282758	0.283106	12.3	1.2
HQ1402_4.dat	120	0.283083	0.283080	1.27E-05	0.001494	7.84E-06	0.065661	1.78E-04	0.008670	1.16E-05	1.487256	0.000102697	43.5	0.282758	0.283079	11.3	0.9
HQ1402_5.dat	120	0.282991	0.283004	1.48E-05	0.001361	5.17E-05	0.038119	1.51E-03	0.008671	1.96E-05	1.487291	0.000120335	44.1	0.282757	0.283003	11.5	1.0
HQ1402_6.dat	30	0.283050	0.283047	2.02E-05	0.001299	1.61E-04	0.059503	5.22E-03	0.008693	2.00E-05	1.487385	0.000262948	42.5	0.282758	0.283046	10.2	1.4
HQ1402_7.dat	60	0.283079	0.283076	1.69E-05	0.000860	3.09E-05	0.044407	1.36E-03	0.008650	1.13E-05	1.487191	0.000109298	43.2	0.282758	0.283075	11.2	1.2
HQ1402_8.dat	120	0.283081	0.283078	1.17E-05	0.001187	2.74E-05	0.053079	1.16E-04	0.008660	9.86E-06	1.487241	0.000130215	43	0.282758	0.283077	11.3	0.9
HQ1402_10.dat	80	0.283084	0.283081	1.59E-05	0.000767	3.59E-05	0.033403	1.80E-04	0.008660	2.23E-05	1.487241	0.000125227	41.6	0.282759	0.283080	11.4	1.1
Median ± 2SD																	

HQ1403 (s080515) n=11																	
HQ1403_1.dat	120	0.283050	0.283047	1.40E-05	0.000743	4.08E-05	0.033480	1.30E-03	0.008676	9.01E-06	1.487228	0.000113482	44.7	0.282757	0.283046	10.2	1.0
HQ1403_2.dat	120	0.283051	0.283048	1.18E-05	0.000556	1.32E-05	0.022288	4.39E-04	0.008679	8.69E-06	1.487251	8.8105E-05	43.7	0.282758	0.283047	10.2	0.8
HQ1403_3.dat	120	0.283074	0.283071	1.49E-05	0.000967	4.00E-05	0.017780	1.94E-04	0.008679	1.96E-05	1.487259	9.7624E-05	43.1	0.282758	0.283037	11.0	1.0
HQ1403_4.dat	70	0.283035	0.283032	1.49E-05	0.001147	6.66E-05	0.049779	2.57E-03	0.008679	1.33E-05	1.487295	0.000128555	42.4	0.282758	0.283031	9.6	1.1
HQ1403_5.dat	120	0.283061	0.283057	1.16E-05	0.001027	5.96E-05	0.040240	1.11E-03	0.008670	9.30E-06	1.487230	8.5014E-05	42.9	0.282758	0.283056	10.6	0.8
HQ1403_6.dat	80	0.283062	0.283059	1.49E-05	0.000960	5.17E-05	0.049624	2.96E-03	0.008669	1.96E-05	1.487291	0.000120335	44.1	0.282758	0.283057	10.7	1.0
HQ1403_7.dat	100	0.283036	0.283033	1.29E-05	0.000775	3.57E-05	0.028650	8.93E-04	0.008655	1.05E-05	1.487286	0.000101488	42.7	0.282758	0.283032	9.7	0.9
HQ1403_9.dat	120	0.283037	0.283033	1.30E-05	0.001134	3.29E-05	0.047810	5.81E-04	0.008674	1.09E-05	1.487230	0.000118214	43.7	0.282758	0.283032	11.5	0.9
HQ1403_10.dat	120	0.283072	0.283068	1.49E-05	0.001088	4.95E-05	0.048715	1.65E-04	0.008674	1.96E-05	1.487252	0.000103052	42.7	0.282758	0.283037	10.8	0.9
HQ1403_11.dat	70	0.283036	0.283033	1.41E-05	0.000780	3.18E-05	0.038087	1.06E-03	0.008664	1.06E-05	1.487228	0.000134107	42.5	0.282758	0.283032	9.7	1.0
HQ1403_12.dat	60	0.283059	0.283056	1.83E-05	0.001063	4.09E-05	0.047855	1.69E-03	0.008671	1.34E-05	1.487231	0.000165233	40.8	0.282759	0.283055	10.5	1.3
Median ± 2SD																	

AG1308A1 (s040215) n=12																	
AG1308A1_10a1	120	0.282956	0.282977	1.24E-05	0.001088	1.02E-05	0.016118	3.08E-04	0.008678	1.54E-05	1.487285	0.00011323	38	0.282761	0.282976	7.6	0.9
AG1308A1_09a1	120	0.282930	0.282951	1.09E-05	0.001665	2.46E-05	0.079308	2.03E-03	0.008650	1.76E-05	1.487331	0.000141319	37.1	0.282762	0.282950	6.7	1.1
AG1308A1_09	120	0.282818	0.282839	1.83E-05	0.001287	4.80E-05	0.078975	2.48E-03	0.008627	2.41E-05	1.487558	0.000157118	37.1	0.282762	0.282838	2.7	1.3
AG1308A1_08a1	120	0.283002	0.283024	2.19E-05	0.001298	3.54E-05	0.059889	1.07E-03	0.008671	2.29E-05	1.487295	0.000131132	38	0.282761	0.283023	9.3	1.5
AG1308A1_07a1	120	0.282987	0.282994	1.82E-05	0.000960	4.95E-05	0.048819	1.21E-04	0.008674	1.96E-05	1.487291	0.000116163	38.7	0.282761	0.282993	8.7	1.0
AG1308A1_06a1	80	0.282994	0.283015	2.34E-05	0.001243	3.26E-05	0.039373	1.25E-04	0.008697	2.99E-05	1.487347	0.000120501	36.8	0.282762	0.283014	8.9	1.7
AG1308A1_05a1	120	0.282978	0.282999	1.45E-05	0.000812	3.68E-06	0.030874	1.49E-04	0.008656	1.02E-05	1.487286	0.000110916	39.3	0.282760	0.282999	8.4	1.0
AG1308A1_04a1	120	0.282980	0.283001	1.49E-05	0.000960												



KJ1302A (s081214) n=13																	
KJ1302A_07a.dat	120	0.282888	0.282997	1.14E-05	0.001027	7.90E-05	0.025242	3.80E-04	0.008662	1.19E-05	1.487222	0.000098	47.0	0.282755	0.282996	8.5	0.8
KJ1302A_21.dat	60	0.283025	0.283048	1.26E-05	0.001233	1.24E-05	0.025242	3.80E-04	0.008662	1.19E-05	1.487222	0.000098	31.0	0.282756	0.283000	8.3	1.2
KJ1302A_07b.dat	120	0.283006	0.283015	1.02E-05	0.001308	1.58E-04	0.025071	2.50E-03	0.008651	1.20E-05	1.487208	0.000097	29.3	0.282767	0.283015	8.8	1.0
KJ1302A_15.dat	120	0.283039	0.283048	1.02E-05	0.000626	1.47E-05	0.016111	2.37E-04	0.008662	8.43E-06	1.487223	0.000086	27.2	0.282768	0.283048	9.9	0.7
KJ1302A_22.dat	120	0.283036	0.283045	1.34E-05	0.000802	3.30E-05	0.022251	3.12E-04	0.008656	1.03E-05	1.487251	0.000108	27.0	0.282768	0.283045	9.8	0.3
KJ1302A_10a.dat	80	0.283009	0.283017	1.97E-05	0.000782	1.46E-05	0.026725	3.31E-04	0.008655	2.13E-05	1.487199	0.000154	27.0	0.282768	0.283018	8.8	1.4
KJ1302A_13.dat	120	0.283038	0.283047	1.19E-05	0.000914	3.19E-05	0.024754	4.81E-04	0.008668	1.14E-05	1.487239	0.000096	26.8	0.282768	0.283047	9.8	0.8
KJ1302A_05a.dat	80	0.283006	0.283014	1.02E-05	0.000856	1.45E-05	0.025165	3.54E-04	0.008652	1.78E-05	1.487264	0.000150	26.8	0.282768	0.283015	9.7	1.1
KJ1302A_20a.dat	70	0.283012	0.283022	2.81E-05	0.000696	2.47E-05	0.023900	5.82E-04	0.008648	3.46E-05	1.487311	0.000281	26.6	0.282768	0.283021	8.9	2.0
KJ1302A_09a.dat	120	0.283027	0.283037	1.03E-05	0.000683	1.71E-05	0.020093	3.92E-04	0.008663	7.40E-06	1.487219	0.000090	26.5	0.282768	0.283036	9.5	0.7
KJ1302A_23a.dat	105	0.283054	0.283063	1.34E-05	0.000958	3.70E-05	0.025559	5.65E-04	0.008661	9.88E-06	1.487314	0.000148	26.5	0.282768	0.283044	10.4	0.9
KJ1302A_18a.dat	120	0.283035	0.283044	1.06E-05	0.000816	1.33E-05	0.020741	1.43E-04	0.008645	9.97E-06	1.487225	0.000091	26.4	0.282768	0.283044	9.7	0.8
KJ1302A_17a.dat	85	0.283044	0.283054	2.09E-05	0.001193	1.05E-04	0.045559	2.74E-03	0.008662	2.11E-05	1.487355	0.000137	26.4	0.282768	0.283053	10.1	1.5
Median ± 2SD													26.4	0.282768	0.283030	9.7	1.3
KJ1303A1 (s081214) n=12																	
KJ1303A2_03a.dat	90	0.283021	0.283031	1.32E-05	0.001056	4.34E-05	0.026436	3.89E-04	0.008670	1.02E-05	1.487340	0.000095	26.6	0.282768	0.283030	9.3	0.9
KJ1303A2_05a.dat	60	0.283010	0.283019	1.97E-05	0.001426	4.72E-05	0.025242	3.80E-04	0.008662	2.48E-05	1.487389	0.000251	26.6	0.282768	0.283019	8.9	1.4
KJ1303A1_09a.dat	90	0.283048	0.283057	1.51E-05	0.000526	1.50E-05	0.021635	3.97E-04	0.008660	1.52E-05	1.487209	0.000122	26.1	0.282769	0.283057	10.2	1.1
KJ1303A2_04a.dat	50	0.283039	0.283048	2.09E-05	0.000400	7.61E-06	0.014189	1.46E-04	0.008666	2.25E-05	1.487511	0.000270	26.0	0.282769	0.283048	9.9	1.5
KJ1303A1_11a.dat	120	0.283046	0.283055	1.25E-05	0.000333	3.02E-06	0.011651	3.50E-05	0.008659	9.07E-06	1.487241	0.000097	25.4	0.282769	0.283055	10.1	0.9
KJ1303A1_10a.dat	80	0.283036	0.283046	2.41E-05	0.000465	1.09E-05	0.017467	2.70E-04	0.008662	1.93E-05	1.487314	0.000148	25.7	0.282769	0.283045	9.8	1.7
KJ1303A1_08a.dat	120	0.283019	0.283028	1.89E-05	0.001159	1.04E-04	0.045359	2.15E-03	0.008650	1.51E-05	1.487266	0.000104	25.6	0.282769	0.283027	9.1	1.3
KJ1303A1_03a.dat	120	0.283048	0.283058	1.19E-05	0.000876	2.27E-05	0.030438	2.27E-04	0.008658	9.32E-06	1.487230	0.000094	25.5	0.282769	0.283057	10.2	0.8
KJ1303A1_15a.dat	60	0.283039	0.283048	1.92E-05	0.000419	7.94E-06	0.015942	2.73E-04	0.008654	1.32E-05	1.487290	0.000158	25.5	0.282769	0.283048	9.9	1.4
KJ1303A1_05a.dat	120	0.283043	0.283052	1.98E-05	0.000489	5.57E-06	0.017257	2.46E-04	0.008657	9.34E-06	1.487241	0.000119	25.4	0.282769	0.283052	10.0	1.0
KJ1303A1_13a.dat	120	0.283011	0.283021	1.98E-05	0.000932	4.04E-05	0.035568	8.72E-04	0.008637	1.28E-05	1.487239	0.000123	25.3	0.282769	0.283020	8.9	1.0
KJ1303A1_07a.dat	60	0.283067	0.283077	1.61E-05	0.000388	9.55E-06	0.015072	1.41E-04	0.008676	1.16E-05	1.487206	0.000174	25.1	0.282769	0.283077	10.9	1.1
Median ± 2SD													25.1	0.282769	0.283077	10.9	1.1
MR1401 (s050215) n=10																	
MR1401_01a.dat	110	0.283075	0.283078	1.89E-05	0.000704	1.78E-05	0.028004	3.10E-04	0.008688	1.50E-05	1.487509	0.00037387	24.7	0.282769	0.283078	10.9	1.4
MR1401_02a.dat	110	0.283023	0.283027	1.27E-05	0.000749	7.11E-05	0.026438	3.89E-04	0.008670	1.26E-05	1.487267	0.000126	24.7	0.282769	0.283026	9.2	0.6
MR1401_03a.dat	110	0.283066	0.283070	1.40E-05	0.000580	2.63E-05	0.028004	3.10E-04	0.008676	1.14E-05	1.487320	0.000236	24.6	0.282770	0.283069	10.6	1.0
MR1401_04a.dat	120	0.283069	0.283073	1.22E-05	0.000369	5.34E-06	0.014321	1.01E-04	0.008686	8.53E-06	1.487283	0.000485	24.8	0.282769	0.283073	10.7	0.9
MR1401_05a.dat	120	0.283062	0.283066	1.42E-05	0.000429	1.25E-05	0.018504	1.32E-04	0.008677	1.09E-05	1.487294	0.000184	24.8	0.282770	0.283066	11.5	0.9
MR1401_06a.dat	120	0.283090	0.283094	1.11E-05	0.000624	2.19E-05	0.022931	4.01E-04	0.008660	8.62E-06	1.487242	0.000666	24.8	0.282770	0.283093	11.4	0.8
MR1401_07a.dat	120	0.283088	0.283092	1.14E-05	0.000718	2.22E-06	0.020290	2.05E-04	0.008674	1.10E-05	1.487259	0.000976	25.4	0.282769	0.283092	11.4	0.8
MR1401_08a.dat	120	0.283075	0.283076	1.18E-05	0.000676	1.81E-05	0.027965	3.96E-04	0.008668	9.95E-06	1.487248	0.000195	25.4	0.282769	0.283076	10.9	0.9
MR1401_09a.dat	80	0.283066	0.283099	1.27E-05	0.000682	9.93E-06	0.028020	3.93E-04	0.008689	1.20E-05	1.487320	0.000816	24.5	0.282770	0.283099	11.4	0.8
MR1401_10a.dat	90	0.283093	0.283097	1.25E-05	0.000436	2.33E-05	0.017786	9.38E-04	0.008672	9.81E-06	1.487264	0.000185	24.3	0.282770	0.283097	11.6	1.4
Median ± 2SD													24.3	0.282770	0.283097	11.6	1.4
KJ1307 (s081214) n=13																	
KJ1307_13a.dat	120	0.283067	0.283076	1.21E-05	0.000703	3.22E-05	0.022559	2.00E-04	0.008651	9.65E-06	1.487225	0.000088	31.7	0.282765	0.283076	11.0	0.3
KJ1307_17a.dat	120	0.283048	0.283057	1.15E-05	0.000339	1.23E-06	0.010711	4.88E-05	0.008645	8.31E-06	1.487242	0.000087	25.3	0.282769	0.283057	10.2	0.8
KJ1307_01a.dat	80	0.283066	0.283075	1.32E-05	0.000829	3.71E-05	0.033677	9.29E-04	0.008665	1.14E-05	1.487212	0.000112	24.9	0.282769	0.283075	10.8	0.9
KJ1307_10a.dat	120	0.283052	0.283061	1.26E-05	0.000429	1.25E-05	0.018504	1.32E-04	0.008677	1.09E-05	1.487294	0.000184	24.8	0.282769	0.283061	10.8	0.9
KJ1307_11a.dat	120	0.283038	0.283047	1.11E-05	0.000622	2.55E-05	0.022438	1.05E-04	0.008645	1.05E-05	1.487270	0.000097	24.6	0.282770	0.283047	9.8	0.8
KJ1307_08a.dat	50	0.283032	0.283041	2.04E-05	0.000468	2.73E-05	0.017476	4.58E-04	0.008646	1.44E-05	1.487411	0.000167	24.5	0.282770	0.283041	9.6	1.4
KJ1307_18a.dat	120	0.283056	0.283065	1.42E-05	0.000429	1.25E-05	0.018504	1.32E-04	0.008677	1.09E-05	1.487294	0.000184	24.4	0.282770	0.283065	10.4	0.9
KJ1307_07a.dat	120	0.283065	0.283074	1.01E-05	0.000417	2.34E-05	0.014480	3.83E-04	0.008643	8.76E-06	1.487327	0.000100	24.4	0.282770	0.283074	10.8	0.7
KJ1307_22a.dat	120	0.283056	0.283065	1.29E-05	0.000497	2.24E-06	0.014642	1.12E-05	0.008650	7.67E-06	1.487260	0.000092	24.1	0.282770	0.283065	10.4	0.9
KJ1307_04a.dat	120	0.283052	0.283061	1.26E-05	0.000429	1.25E-05	0.018504	1.32E-04	0.008677	1.09E-05	1.487294	0.000184	24.1	0.282770	0.283061	10.4	0.9
KJ1307_03a.dat	120	0.283051	0.283060	1.06E-05	0.000616	1.61E-06	0.022523	3.72E-04	0.008656	8.18E-06	1.487250	0.000112	23.7	0.282770	0.283060	10.3	0.7
KJ1307_14a.dat	120	0.283042	0.283051	1.14E-05	0.000489	1.28E-05	0.017788	2.73E-04	0.008649	1.02E-05	1.487243	0.000092	23.7	0.282770	0.283051	9.9	0.8
KJ1307_19a.dat	60	0.283057	0.283066	1.43E-05	0.000524	1.44E-05	0.017748	2.94E-04	0.008646	1.13E-05	1.487347	0.000137	23.7	0.282770	0.283066	10.5	1.0
Median ± 2SD													23.7	0.282770	0.283066	10.5	1.0
LI1301 (s040215) n=10																	
LI1301_10a.dat	120	0.283065	0.283068	1.80E-05	0.000846	3.53E-05	0.030299	6.64E-04	0.008677	1.15E-05	1.487247	0.00012112	22.9	0.282771	0.283068	11.1	1.3
LI1301_09a.dat	120	0.283063	0.283084	1.42E-05	0.001034	4.33E-05	0.038022	9.20E-04	0.008680	1.30E-05	1.487267	0.00016236	23.1	0.282770	0.283083	11.1	1.0
LI1301_08a.dat	120	0.283044	0.283048	1.42E-05	0.001044	4.33E-05	0.038022	9.20E-04	0.008680	1.30E-05	1.487267	0.00016236	23.1	0.282770	0.283083	11.1	1.0
LI1301_07a.dat	120	0.283062	0.283063	1.72E-05	0.001004	4.24E-05	0.038022	9.20E-04	0.008680	1.30E-05	1.487267	0.00016236	23.1	0.282770	0.283063	11.1	1.0
LI1301_06a.dat	100	0.283043	0.283065	1.45E-05	0.000800	2.52E-05	0.021142										

STANDARDS															
Analysis (TM: n=8; PL: n=8)	# cycles integrated	176Hu/177Hf	Zse	176Lu/177Hf	Zse	173Yb/177Hf	1se	178Hu/177Hf	Zse	Age (Ma)	176Hu/177Hf CHUR*	176Hu/177Hf (t)	σHf (t)	Zse	σHf offset from ref
<b>S021214</b>															
<b>TEMORA-2 (n=11)</b>															
TM_10-1.dat	120	0.282695	0.000011	0.001104	0.000008	0.039679	0.000157	1.467264	0.000083	417	0.282522	0.282687	5.8	0.8	0.0
TM_10-3.dat	120	0.282704	0.000013	0.001344	0.000005	0.047713	0.000187	1.467244	0.000083	417	0.282522	0.282693	6.1	0.9	0.2
TM_10-4.dat	120	0.282684	0.000012	0.000952	0.000007	0.021806	0.000136	1.467224	0.000086	417	0.282522	0.282679	5.5	0.9	-0.2
TM_10-5.dat	80	0.282689	0.000015	0.000648	0.000018	0.020646	0.000242	1.467281	0.000102	417	0.282522	0.282684	5.7	1.0	-0.1
TM_10-6.dat	120	0.282666	0.000013	0.001221	0.000005	0.042481	0.000073	1.467261	0.000086	417	0.282522	0.282687	4.7	0.9	-1.0
TM_10-7.dat	110	0.282695	0.000013	0.001410	0.000003	0.049623	0.000043	1.467209	0.000084	417	0.282522	0.282674	5.4	0.9	-0.4
TM_10-8.dat	120	0.282682	0.000013	0.001830	0.000029	0.062879	0.000593	1.467313	0.000115	417	0.282522	0.282687	5.1	0.9	-0.6
TM_10-11.dat	120	0.282671	0.000014	0.002196	0.000030	0.074988	0.000421	1.467246	0.000092	417	0.282522	0.282654	4.7	1.0	-1.1
TM_10-12.dat	120	0.282676	0.000014	0.000509	0.000002	0.017410	0.000152	1.467229	0.000082	417	0.282522	0.282672	5.3	1.0	-0.2
TM_10-13.dat	110	0.282671	0.000012	0.000531	0.000005	0.018070	0.000155	1.467236	0.000082	417	0.282522	0.282687	5.1	0.9	-0.6
TM_10-14.dat	90	0.282694	0.000013	0.000540	0.000007	0.018364	0.000156	1.467276	0.000081	417	0.282522	0.282690	5.9	0.9	-0.1
											<b>ZSD</b>	<b>0.000026</b>	<b>0.9</b>		<b>-0.4</b>
											<b>Normalization factor</b>	<b>1.000040</b>			
<b>PLESOVICE (n=12)</b>															
PL_10-2.dat	120	0.282493	0.000012	0.000116	0.000002	0.009596	0.000043	1.467241	0.000132	337	0.282573	0.282482	-2.8	0.8	0.3
PL_10-3.dat	120	0.282489	0.000011	0.000091	0.000001	0.004919	0.000038	1.467292	0.000092	337	0.282573	0.282485	-3.1	0.8	0.1
PL_10-4.dat	120	0.282472	0.000013	0.000091	0.000000	0.004619	0.000033	1.467239	0.000087	337	0.282573	0.282471	-3.6	0.9	-0.4
PL_10-5.dat	120	0.282473	0.000011	0.000133	0.000002	0.009504	0.000026	1.467268	0.000099	337	0.282573	0.282473	-3.6	0.8	-0.3
PL_10-6.dat	120	0.282471	0.000011	0.000091	0.000000	0.004544	0.000023	1.467291	0.000100	337	0.282573	0.282471	-3.6	0.8	-0.4
PL_10-7.dat	120	0.282467	0.000012	0.000122	0.000002	0.005406	0.000025	1.467274	0.000101	337	0.282573	0.282466	-3.8	0.8	-0.5
PL_10-8.dat	120	0.282477	0.000011	0.000128	0.000002	0.008284	0.000021	1.467292	0.000087	337	0.282573	0.282477	-3.4	0.8	-0.2
PL_10-9.dat	120	0.282470	0.000012	0.000128	0.000001	0.006186	0.000016	1.467297	0.000085	337	0.282573	0.282469	-3.7	0.9	-0.4
PL_10-10.dat	120	0.282475	0.000012	0.000128	0.000001	0.005189	0.000018	1.467290	0.000084	337	0.282573	0.282475	-3.5	0.8	-0.2
PL_10-11.dat	120	0.282467	0.000010	0.000128	0.000001	0.008250	0.000018	1.467237	0.000086	337	0.282573	0.282466	-3.9	0.7	-0.5
PL_10-12.dat	120	0.282468	0.000012	0.000130	0.000001	0.006340	0.000019	1.467297	0.000088	337	0.282573	0.282468	-3.7	0.8	-0.5
PL_10-13.dat	120	0.282484	0.000010	0.000128	0.000001	0.006283	0.000022	1.467273	0.000077	337	0.282573	0.282483	-3.2	0.7	0.0
											<b>Mean</b>	<b>0.282475</b>	<b>-3.5</b>		<b>-0.2</b>
											<b>ZSD</b>	<b>0.000016</b>	<b>0.6</b>		
											<b>Normalization factor</b>	<b>1.000026</b>			
											<b>Average Normalization factor (TM + PL)</b>	<b>1.000033</b>			
<b>S020315</b>															
<b>TEMORA-2 (n=6)</b>															
TM_14-06.dat	120	0.282661	0.000010	0.001286	0.000042	0.051175	0.000713	1.467281	0.000074	417	0.282522	0.282681	4.6	0.7	-1.2
TM_14-05.dat	90	0.282671	0.000011	0.000841	0.000010	0.027281	0.000028	1.467296	0.000089	417	0.282522	0.282686	5.1	0.8	-0.7
TM_14-04.dat	120	0.282671	0.000010	0.000864	0.000015	0.028029	0.000036	1.467273	0.000087	417	0.282522	0.282686	5.1	0.7	-0.7
TM_14-03.dat	120	0.282659	0.000010	0.001376	0.000013	0.054626	0.000316	1.467291	0.000075	417	0.282522	0.282688	4.4	0.7	-1.3
TM_14-02.dat	120	0.282673	0.000010	0.001028	0.000020	0.043601	0.000057	1.467275	0.000081	417	0.282522	0.282685	5.0	0.7	-0.7
TM_14-01.dat	120	0.282667	0.000011	0.001038	0.000024	0.042866	0.000034	1.467294	0.000071	417	0.282522	0.282689	4.5	0.7	-1.2
											<b>Mean</b>	<b>0.282657</b>	<b>4.8</b>		<b>-1.0</b>
											<b>ZSD</b>	<b>0.000018</b>	<b>0.6</b>		
											<b>Normalization factor</b>	<b>1.000101</b>			
<b>PLESOVICE (n=6)</b>															
PL_14-05.dat	120	0.282473	0.000009	0.000127	0.000001	0.008157	0.000019	1.467294	0.000064	337	0.282573	0.282472	-3.6	0.6	-0.3
PL_14-05.dat	120	0.282472	0.000010	0.000128	0.000001	0.007959	0.000019	1.467283	0.000076	337	0.282573	0.282472	-3.6	0.7	-0.3
PL_14-04.dat	120	0.282473	0.000009	0.000128	0.000001	0.007993	0.000021	1.467294	0.000093	337	0.282573	0.282478	-3.4	0.6	-0.1
PL_14-03.dat	120	0.282468	0.000009	0.000128	0.000001	0.007881	0.000019	1.467295	0.000073	337	0.282573	0.282468	-3.7	0.7	-0.5
PL_14-02.dat	120	0.282465	0.000010	0.000129	0.000001	0.008005	0.000023	1.467294	0.000085	337	0.282573	0.282465	-3.8	0.7	-0.6
PL_14-01.dat	120	0.282478	0.000010	0.000112	0.000002	0.007527	0.000054	1.467305	0.000074	337	0.282573	0.282477	-3.4	0.7	-0.2
											<b>Mean</b>	<b>0.282472</b>	<b>-3.8</b>		<b>-0.3</b>
											<b>ZSD</b>	<b>0.000011</b>	<b>0.4</b>		
											<b>Normalization factor</b>	<b>1.000036</b>			
											<b>Average Normalization factor (TM + PL)</b>	<b>1.000069</b>			
<b>S040215</b>															
<b>TEMORA-2 (n=8)</b>															
TM_6-4.dat	120	0.282677	0.000011	0.001612	0.000016	0.064218	0.000263	1.467298	0.000091	417	0.282522	0.282684	5.0	0.8	-0.7
TM_6-3.dat	100	0.282657	0.000011	0.001360	0.000032	0.050297	0.000592	1.467284	0.000085	417	0.282522	0.282647	4.4	0.8	-1.3
TM_6-2.dat	100	0.282669	0.000012	0.001453	0.000052	0.056158	0.000870	1.467304	0.000088	417	0.282522	0.282658	4.8	0.8	-0.9
TM_6-1.dat	100	0.282675	0.000011	0.001568	0.000037	0.057178	0.000592	1.467302	0.000077	417	0.282522	0.282662	5.0	0.8	-0.8
TM_5-4.dat	120	0.282666	0.000012	0.000669	0.000005	0.027633	0.000214	1.467287	0.000112	417	0.282522	0.282661	4.9	0.9	-0.8
TM_5-3.dat	120	0.282668	0.000012	0.001351	0.000020	0.059849	0.000635	1.467294	0.000083	417	0.282522	0.282667	4.9	0.9	-1.0
TM_5-2.dat	120	0.282662	0.000013	0.001084	0.000011	0.045866	0.000350	1.467321	0.000091	417	0.282522	0.282654	4.7	0.9	-1.1
TM_5-1.dat	120	0.282663	0.000015	0.001598	0.000016	0.072868	0.000438	1.467284	0.000114	417	0.282522	0.282650	4.5	1.1	-1.2
											<b>Mean</b>	<b>0.282657</b>	<b>4.8</b>		<b>-1.0</b>
											<b>ZSD</b>	<b>0.000012</b>	<b>0.4</b>		
											<b>Normalization factor</b>	<b>1.000104</b>			
<b>PLESOVICE (n=10)</b>															
PL_6-5.dat	120	0.282464	0.000011	0.000163	0.000001	0.011833	0.000095	1.467292	0.000103	337	0.282573	0.282463	-3.9	0.8	-0.6
PL_6-4.dat	120	0.282464	0.000011	0.000097	0.000001	0.006162	0.000055	1.467268	0.000083	337	0.282573	0.282464	-3.9	0.8	-0.6
PL_6-3.dat	120	0.282475	0.000013	0.000092	0.000001	0.006049	0.000030	1.467303	0.000086	337	0.282573	0.282475	-3.5	0.9	-0.2
PL_6-2.dat	120	0.282478	0.000010	0.000074	0.000002	0.004548	0.000056	1.467292	0.000070	337	0.282573	0.282477	-3.4	0.7	-0.2
PL_6-1.dat	120	0.282480	0.000011	0.000076	0.000001	0.004447	0.000030	1.467267	0.000075	337	0.282573	0.282479	-3.3	0.8	-0.1
PL_5-6.dat	120	0.282470	0.000013	0.000067	0.000002	0.004327	0.000040	1.467294	0.000082	337	0.282573	0.282470	-3.6		

s080515															
<b>TEMORA-2 (n=24)</b>															
TM-NW_13_1.dat	90	0.282698	0.000012	0.001226	0.000022	0.065550	0.001703	1.467234	0.000127	417	0.282522	0.282688	5.9	0.9	0.1
TM-NW_13_2.dat	100	0.282713	0.000018	0.001328	0.000031	0.073036	0.001563	1.467294	0.000100	417	0.282522	0.282703	6.4	1.3	0.6
TM-NW_13_3.dat	110	0.282670	0.000017	0.001449	0.000048	0.076968	0.000599	1.467295	0.000089	417	0.282522	0.282682	6.0	1.1	0.2
TM-NW_13_4.dat	110	0.282716	0.000018	0.001559	0.000050	0.056145	0.001525	1.467296	0.000112	417	0.282522	0.282708	6.6	1.3	0.7
TM-NW_13_5.dat	110	0.282680	0.000018	0.001375	0.000013	0.078925	0.000957	1.467296	0.000115	417	0.282522	0.282669	5.2	1.3	-0.6
TM-NW_13_6.dat	120	0.282673	0.000015	0.001369	0.000011	0.076744	0.000926	1.467297	0.000121	417	0.282522	0.282682	4.9	1.0	-0.8
TM-NW_13_7.dat	110	0.282664	0.000017	0.001449	0.000010	0.069119	0.000401	1.467288	0.000090	417	0.282522	0.282633	3.9	1.2	-1.8
TM-NW_13_8.dat	110	0.282674	0.000014	0.001454	0.000012	0.059566	0.000325	1.467340	0.000103	417	0.282522	0.282683	5.0	1.0	-0.8
TM-NW_13_9.dat	110	0.282704	0.000018	0.001495	0.000013	0.071853	0.000460	1.467298	0.000089	417	0.282522	0.282692	6.0	1.1	0.2
TM-NW_13_10.dat	120	0.282665	0.000018	0.001470	0.000012	0.071229	0.000558	1.467278	0.000094	417	0.282522	0.282673	5.3	1.2	-0.4
TM-NW_13_11.dat	120	0.282680	0.000015	0.001383	0.000039	0.065565	0.000668	1.467281	0.000086	417	0.282522	0.282669	5.2	1.1	-0.6
TM-NW_13_12.dat	120	0.282707	0.000015	0.001408	0.000039	0.067239	0.000647	1.467285	0.000080	417	0.282522	0.282686	6.1	1.1	0.3
TM-NW_13_13.dat	120	0.282655	0.000019	0.001622	0.000022	0.062488	0.000347	1.467254	0.000079	417	0.282522	0.282642	4.2	1.4	-1.5
TM-NW_13_14.dat	120	0.282681	0.000017	0.001622	0.000099	0.079273	0.003326	1.467254	0.000083	417	0.282522	0.282669	5.2	1.2	-0.6
TM-NW_13_15.dat	120	0.282704	0.000016	0.001624	0.000015	0.078641	0.001211	1.467194	0.000095	417	0.282522	0.282691	6.0	1.1	0.2
TM-NW_13_16.dat	120	0.282687	0.000018	0.001400	0.000021	0.067855	0.000678	1.467291	0.000080	417	0.282522	0.282676	5.4	1.3	-0.3
TM-NW_13_17.dat	120	0.282717	0.000017	0.001313	0.000009	0.064649	0.000678	1.467286	0.000094	417	0.282522	0.282707	6.5	1.2	0.7
TM-NW_13_18.dat	120	0.282679	0.000018	0.001180	0.000016	0.060036	0.001507	1.467244	0.000108	417	0.282522	0.282664	5.0	1.3	-0.7
TM-NW_13_19.dat	120	0.282705	0.000019	0.002422	0.000069	0.118372	0.002095	1.467251	0.000103	417	0.282522	0.282686	5.8	1.3	0.0
TM-NW_13_20.dat	120	0.282705	0.000017	0.000542	0.000003	0.025273	0.000395	1.467265	0.000101	417	0.282522	0.282705	6.5	1.2	0.6
TM-NW_13_21.dat	120	0.282718	0.000016	0.000627	0.000025	0.029889	0.000385	1.467296	0.000099	417	0.282522	0.282714	6.8	1.1	0.9
TM-NW_13_22.dat	120	0.282713	0.000015	0.000568	0.000005	0.024535	0.000225	1.467296	0.000103	417	0.282522	0.282709	6.6	1.0	0.8
TM-NW_13_23.dat	120	0.282707	0.000015	0.000525	0.000001	0.023168	0.000200	1.467285	0.000109	417	0.282522	0.282703	6.4	1.1	0.6
TM-NW_13_24.dat	120	0.282717	0.000015	0.000549	0.000001	0.023970	0.000234	1.467219	0.000110	417	0.282522	0.282717	6.9	1.0	1.0
											Mean	0.282683	5.7		-4.1
											SD	0.000046	1.6		
											Normalization factor	1.000010			
<b>PLESIOVICE (n=18)</b>															
PL-NW_13_1.dat	110	0.282479	0.000014	0.000130	0.000004	0.008208	0.000098	1.467289	0.000116	337	0.282573	0.282478	-3.3	1.0	-0.1
PL-NW_13_2.dat	110	0.282488	0.000013	0.000074	0.000004	0.004805	0.000106	1.467338	0.000088	337	0.282573	0.282487	-3.0	0.9	0.2
PL-NW_13_3.dat	110	0.282494	0.000013	0.000068	0.000004	0.004441	0.000095	1.467304	0.000099	337	0.282573	0.282474	-2.8	0.9	0.4
PL-NW_13_4.dat	110	0.282475	0.000014	0.000070	0.000005	0.004058	0.000116	1.467304	0.000109	337	0.282573	0.282474	-3.5	1.0	-0.3
PL-NW_13_5.dat	110	0.282482	0.000013	0.000064	0.000003	0.003943	0.000073	1.467304	0.000103	337	0.282573	0.282482	-2.9	0.9	0.3
PL-NW_13_6.dat	120	0.282472	0.000015	0.000063	0.000002	0.004202	0.000054	1.467273	0.000082	337	0.282573	0.282472	-3.6	1.0	-0.3
PL-NW_13_7.dat	120	0.282476	0.000013	0.000065	0.000003	0.004375	0.000084	1.467257	0.000095	337	0.282573	0.282476	-3.4	0.9	-0.2
PL-NW_13_8.dat	120	0.282483	0.000013	0.000065	0.000003	0.004481	0.000076	1.467296	0.000093	337	0.282573	0.282483	-3.2	0.9	0.0
PL-NW_13_9.dat	120	0.282490	0.000013	0.000062	0.000003	0.004300	0.000080	1.467296	0.000103	337	0.282573	0.282490	-3.6	1.0	-1.2
PL-NW_13_10.dat	120	0.282479	0.000015	0.000067	0.000003	0.004430	0.000071	1.467287	0.000090	337	0.282573	0.282479	-3.3	1.0	-0.1
PL-NW_13_11.dat	120	0.282489	0.000014	0.000088	0.000005	0.005489	0.000124	1.467240	0.000100	337	0.282573	0.282489	-3.0	1.0	0.2
PL-NW_13_12.dat	120	0.282484	0.000014	0.000081	0.000004	0.005113	0.000079	1.467291	0.000097	337	0.282573	0.282484	-3.1	0.9	0.1
PL-NW_13_13.dat	120	0.282506	0.000013	0.000128	0.000004	0.008131	0.000078	1.467253	0.000099	337	0.282573	0.282506	-2.4	0.9	0.8
PL-NW_13_14.dat	120	0.282529	0.000013	0.000134	0.000002	0.008618	0.000116	1.467267	0.000094	337	0.282573	0.282508	-2.3	1.0	0.9
PL-NW_13_15.dat	120	0.282495	0.000014	0.000142	0.000003	0.009113	0.000103	1.467291	0.000103	337	0.282573	0.282495	-2.7	0.9	0.4
PL-NW_13_16.dat	120	0.282505	0.000012	0.000144	0.000001	0.009191	0.000074	1.467242	0.000102	337	0.282573	0.282504	-2.4	0.9	0.7
PL-NW_13_17.dat	120	0.282521	0.000012	0.000130	0.000002	0.008951	0.000110	1.467231	0.000103	337	0.282573	0.282520	-1.9	0.8	1.3
PL-NW_13_18.dat	120	0.282525	0.000013	0.000121	0.000005	0.007835	0.000110	1.467243	0.000102	337	0.282573	0.282524	-1.7	0.9	1.4
											Mean	0.282491	-2.9		0.3
											SD	0.000001	1.1		
											Normalization factor	0.999986			
											Average Normalization factor (TM + PL)	0.999988			
<b>s07-081015</b>															
<b>TEMORA-2 (n=19)</b>															
TM_12-1.dat	120	0.282668	0.000014	0.001882	0.000008	0.088149	0.000499	1.467330	0.000101	417	0.282522	0.282653	4.6	1.0	-1.1
TM_12-2.dat	120	0.282669	0.000012	0.001500	0.000006	0.080877	0.000415	1.467316	0.000100	417	0.282522	0.282667	4.8	0.9	-1.0
TM_12-3.dat	120	0.282663	0.000015	0.001538	0.000006	0.087717	0.000150	1.467354	0.000111	417	0.282522	0.282651	4.6	1.0	-1.2
TM_12-4.dat	120	0.282659	0.000014	0.001601	0.000024	0.074211	0.000862	1.467330	0.000099	417	0.282522	0.282646	4.4	1.0	-1.3
TM_12-5.dat	95	0.282684	0.000016	0.002057	0.000031	0.119238	0.001033	1.467348	0.000111	417	0.282522	0.282664	5.0	1.1	-0.7
TM_12-6.dat	120	0.282692	0.000015	0.002042	0.000017	0.114623	0.000923	1.467340	0.000117	417	0.282522	0.282660	5.0	1.1	-0.2
TM_12-7.dat	120	0.282685	0.000014	0.002021	0.000014	0.103791	0.000265	1.467334	0.000081	417	0.282522	0.282679	5.5	1.0	-0.2
TM_12-8.dat	120	0.282696	0.000014	0.002079	0.000018	0.104481	0.000413	1.467298	0.000124	417	0.282522	0.282689	5.9	1.0	0.1
TM_12-9.dat	120	0.282696	0.000012	0.002022	0.000021	0.102638	0.000337	1.467298	0.000083	417	0.282522	0.282691	5.3	1.1	-0.1
TM_12-10.dat	120	0.282666	0.000015	0.001332	0.000037	0.065632	0.000859	1.467323	0.000105	417	0.282522	0.282655	4.7	1.1	-1.0
TM_12-11.dat	120	0.282707	0.000019	0.001501	0.000029	0.062704	0.000545	1.467260	0.000170	417	0.282522	0.282695	6.1	1.3	0.3
TM_12-12.dat	120	0.282693	0.000012	0.001192	0.000046	0.052622	0.001185	1.467325	0.000080	417	0.282522	0.282664	4.7	0.9	-1.1
TM_12-13.dat	120	0.282697	0.000014	0.001643	0.000079	0.076062	0.000243	1.467318	0.000111	417	0.282522	0.282644	4.3	1.0	-0.4
TM_12-14.dat	120	0.282677	0.000014	0.001513	0.000015	0.068160									

**PLESOVICE (n=28)**

run1PL_2-1.da	120	0.282474	0.000006	0.000112	0.000001	0.008151	0.000028	1.467235	0.000078	337	0.282573	0.282473	-3.5	0.5	-0.3
run1PL_2-2.da	120	0.282469	0.000007	0.000062	0.000000	0.004873	0.000006	1.467255	0.000074	337	0.282573	0.282468	-3.7	0.5	-0.5
run1PL_2-3.da	120	0.282480	0.000007	0.000062	0.000000	0.004884	0.000017	1.467259	0.000077	337	0.282573	0.282480	-3.3	0.5	-0.1
run1PL_2-4.da	120	0.282464	0.000007	0.000072	0.000001	0.005121	0.000050	1.467209	0.000074	337	0.282573	0.282463	-3.9	0.5	-0.6
run1PL_2-5.da	120	0.282472	0.000007	0.000098	0.000000	0.006861	0.000038	1.467229	0.000089	337	0.282573	0.282472	-3.6	0.5	-0.3
run1PL_2-6.da	120	0.282487	0.000007	0.000090	0.000001	0.005455	0.000049	1.467254	0.000081	337	0.282573	0.282486	-3.1	0.5	0.1
run1PL_2-7.da	120	0.282486	0.000006	0.000083	0.000001	0.005903	0.000057	1.467246	0.000069	337	0.282573	0.282486	-3.1	0.5	0.1
run1PL_2-8.da	120	0.282485	0.000008	0.000091	0.000003	0.005827	0.000120	1.467218	0.000077	337	0.282573	0.282485	-3.1	0.6	0.1
run1PL_2-9.da	120	0.282478	0.000008	0.000103	0.000000	0.007416	0.000024	1.467233	0.000066	337	0.282573	0.282477	-3.4	0.5	-0.2
run1PL_2-10.d	120	0.282478	0.000007	0.000103	0.000000	0.007321	0.000024	1.467234	0.000076	337	0.282573	0.282478	-3.4	0.5	-0.1
run1PL_2-11.d	120	0.282478	0.000007	0.000105	0.000000	0.007841	0.000022	1.467241	0.000062	337	0.282573	0.282478	-3.4	0.5	-0.1
run1PL_2-12.d	120	0.282478	0.000007	0.000105	0.000000	0.007703	0.000114	1.467253	0.000075	337	0.282573	0.282477	-3.4	0.5	-0.2
run1PL_2-13.d	120	0.282469	0.000007	0.000111	0.000002	0.007784	0.000047	1.467245	0.000087	337	0.282573	0.282468	-3.7	0.5	-0.5
run1PL_2-14.d	120	0.282480	0.000007	0.000116	0.000002	0.008378	0.000080	1.467265	0.000078	337	0.282573	0.282479	-3.3	0.5	-0.1
run1PL_2-15.d	120	0.282485	0.000007	0.000100	0.000002	0.006862	0.000068	1.467243	0.000079	337	0.282573	0.282485	-3.1	0.5	0.1
run1PL_2-1.da	120	0.282472	0.000006	0.000117	0.000001	0.009016	0.000030	1.467225	0.000106	337	0.282573	0.282471	-3.6	0.4	-0.4
run2PL_2-2.da	120	0.282473	0.000008	0.000114	0.000000	0.008864	0.000032	1.467167	0.000066	337	0.282573	0.282473	-3.5	0.6	-0.3
run2PL_2-3.da	120	0.282472	0.000007	0.000101	0.000000	0.007772	0.000072	1.467215	0.000118	337	0.282573	0.282471	-3.6	0.5	-0.4
run2PL_2-4.da	120	0.282476	0.000005	0.000126	0.000000	0.008610	0.000020	1.467226	0.000080	337	0.282573	0.282475	-3.5	0.4	-0.2
run2PL_2-5.da	120	0.282469	0.000006	0.000126	0.000000	0.008917	0.000042	1.467218	0.000144	337	0.282573	0.282468	-3.7	0.4	-0.5
run2PL_2-6.da	120	0.282469	0.000005	0.000130	0.000000	0.008824	0.000038	1.466837	0.000089	337	0.282573	0.282468	-3.7	0.4	-0.5
run2PL_2-7.da	120	0.282475	0.000004	0.000148	0.000001	0.010291	0.000041	1.467230	0.000069	337	0.282573	0.282474	-3.5	0.3	-0.3
run2PL_2-8.da	120	0.282470	0.000007	0.000130	0.000000	0.009729	0.000032	1.466661	0.000072	337	0.282573	0.282469	-3.7	0.5	-0.4
run2PL_1-11.da	120	0.282466	0.000008	0.000068	0.000002	0.004627	0.000060	1.467236	0.000068	337	0.282573	0.282468	-3.7	0.6	-0.5
run2PL_1-21.da	120	0.282475	0.000007	0.000068	0.000002	0.004540	0.000075	1.467219	0.000077	337	0.282573	0.282475	-3.5	0.5	-0.2
run2PL_1-33.da	120	0.282466	0.000008	0.000070	0.000002	0.004803	0.000068	1.467246	0.000062	337	0.282573	0.282465	-3.8	0.5	-0.6
run2PL_1-4.da	120	0.282475	0.000007	0.000062	0.000002	0.004560	0.000052	1.467259	0.000073	337	0.282573	0.282475	-3.5	0.5	-0.2
run2PL_1-5.da	75	0.282471	0.000008	0.000058	0.000002	0.004035	0.000052	1.467245	0.000086	337	0.282573	0.282470	-3.6	0.6	-0.4

**Mean** 0.282474 -3.5 -0.3  
**ZSD** 0.000012 0.4  
**Normalization factor** 1.000008  
**Average Normalization factor (TM = P)** 1.000056





Table DR5: Results of in situ SIMS oxygen isotope analyses.

Analysis (n=280)	Spot location single grain	$^{18}\text{O}/^{16}\text{O}$	1 $\sigma$ (%) Inter-session	$\delta^{18}\text{O}$ (SMOW)	2 $\sigma$ (‰) Inter-session
<b>AG1304A (n=20)</b>					
AG1304A_1/1	Core	0.00201580	0.0099	5.28	0.20
AG1304A_11/1	Core	0.00201578	0.0095	5.28	0.19
AG1304A_11/2	Rim	0.00201589	0.0094	5.33	0.19
AG1304A_12/1	Core	0.00201546	0.0111	5.12	0.22
AG1304A_12/2	Rim	0.00201546	0.0094	5.12	0.19
AG1304A_13/1	Core	0.00201557	0.0076	5.17	0.15
AG1304A_13/2	Rim	0.00201548	0.0107	5.13	0.21
AG1304A_18/1	Core	0.00201566	0.0118	5.21	0.24
AG1304A_18/2	Rim	0.00201586	0.0114	5.32	0.23
AG1304A_25/1	Core	0.00201583	0.0099	5.30	0.20
AG1304A_25/2	Rim	0.00201533	0.0106	5.05	0.21
AG1304A_30/1	Core	0.00201556	0.0108	5.16	0.22
AG1304A_4/1	Core	0.00201511	0.0084	4.94	0.17
AG1304A_4/2	Intermediate	0.00201552	0.0085	5.15	0.17
AG1304A_4/3	Rim	0.00201579	0.0077	5.28	0.15
AG1304A_17/1	Core	0.00201571	0.0081	5.24	0.16
AG1304A_17/2	Rim	0.00201558	0.0108	5.18	0.22
AG1304A_32/1	Core	0.00201576	0.0097	5.26	0.19
AG1304A_32/2	Rim	0.00201573	0.0080	5.25	0.16
AG1304A_5/1	Core	0.00201560	0.0079	5.19	0.16
<b>Median <math>\pm</math> 2SD</b>				<b>5.20</b>	<b>0.19</b>
<b>AG1401 (n=20)</b>					
AG1401_1/1	Core	0.00201376	0.0122	4.27	0.24
AG1401_1/2	Rim	0.00201358	0.0079	4.18	0.16
AG1401_11/1	Core	0.00201396	0.0118	4.37	0.24
AG1401_11/2	Intermediate	0.00201368	0.0089	4.23	0.18
AG1401_11/3	Rim	0.00201444	0.0098	4.61	0.20
AG1401_16/1	Core	0.00201361	0.0114	4.20	0.23
AG1401_17/1	Core	0.00201559	0.0076	5.18	0.15
AG1401_17/2	Intermediate	0.00201550	0.0113	5.13	0.23
AG1401_17/3	Rim	0.00201509	0.0082	4.93	0.16
AG1401_3/1	Core	0.00201384	0.0096	4.31	0.19
AG1401_3/2	Rim	0.00201499	0.0101	4.88	0.20

AG1401_7/1	Core	0.00201491	0.0098	4.84	0.20
AG1401_10/1	Core	0.00201394	0.0104	4.36	0.21
AG1401_13/1	Core	0.00201406	0.0081	4.42	0.16
AG1401_13/2	Rim	0.00201452	0.0084	4.65	0.17
AG1401_18/1	Core	0.00201374	0.0083	4.26	0.17
AG1401_22/1	Core	0.00201373	0.0090	4.25	0.18
AG1401_22/2	Rim	0.00201472	0.0112	4.75	0.22
AG1401_6/1	Core	0.00201547	0.0102	5.12	0.20
AG1401_6/2	Rim	0.00201494	0.0083	4.86	0.17
<b>Median ± 2SD</b>				<b>4.51</b>	<b>0.69</b>
<b>AG1402 (n=20)</b>					
AG1402_1/1	Core	0.00201614	0.0077	5.46	0.15
AG1402_1/2	Rim	0.00201561	0.0113	5.19	0.23
AG1402_18/1	Core	0.00201634	0.0098	5.56	0.20
AG1402_18/2	Rim	0.00201600	0.0095	5.39	0.19
AG1402_3/1	Core	0.00201598	0.0104	5.38	0.21
AG1402_3/2	Rim	0.00201583	0.0101	5.30	0.20
AG1402_6/1	Core	0.00201576	0.0096	5.27	0.19
AG1402_6/2	Rim	0.00201586	0.0107	5.32	0.21
AG1402_9/1	Core	0.00201609	0.0078	5.43	0.16
AG1402_9/2	Intermediate	0.00201578	0.0101	5.28	0.20
AG1402_9/3	Rim	0.00201589	0.0101	5.33	0.20
AG1402_10/1	Core	0.00201593	0.0089	5.35	0.18
AG1402_14/1	Core	0.00201587	0.0085	5.32	0.17
AG1402_16/1	Core	0.00201587	0.0075	5.32	0.15
AG1402_19/1	Core	0.00201580	0.0102	5.29	0.20
AG1402_19/2	Intermediate	0.00201597	0.0079	5.37	0.16
AG1402_19/3	Rim	0.00201572	0.0088	5.24	0.18
AG1402_22/1	Core	0.00201584	0.0099	5.30	0.20
AG1402_8/1	Core	0.00201585	0.0087	5.31	0.17
AG1402_8/2	Rim	0.00201592	0.0096	5.35	0.19
<b>Median ± 2SD</b>				<b>5.32</b>	<b>0.16</b>
<b>HQ1403 (n=20)</b>					
HQ1403_1/1	Core	0.00201615	0.0086	5.46	0.17
HQ1403_1/2	Rim	0.00201553	0.0117	5.15	0.23
HQ1403_11/1	Core	0.00201611	0.0106	5.44	0.21
HQ1403_11/2	Rim	0.00201605	0.0106	5.41	0.21
HQ1403_12/1	Core	0.00201643	0.0108	5.60	0.22
HQ1403_17/1	Core	0.00201606	0.0133	5.42	0.27
HQ1403_17/2	Rim	0.00201604	0.0076	5.41	0.15
HQ1403_2/1	Core	0.00201600	0.0106	5.39	0.21
HQ1403_2/2	Rim	0.00201575	0.0113	5.26	0.23
HQ1403_22/1	Core	0.00201574	0.0112	5.25	0.22
HQ1403_3/1	Core	0.00201595	0.0112	5.36	0.22
HQ1403_4/1	Core	0.00201614	0.0104	5.46	0.21
HQ1403_7/1	Core	0.00201632	0.0099	5.55	0.20
HQ1403_15/1	Core	0.00201698	0.0098	5.87	0.20
HQ1403_15/2	Rim	0.00201581	0.0093	5.29	0.19
HQ1403_16/1	Core	0.00201616	0.0082	5.47	0.16
HQ1403_16/2	Rim	0.00201631	0.0098	5.54	0.20
HQ1403_18/1	Core	0.00201601	0.0075	5.39	0.15
HQ1403_20/1	Core	0.00201609	0.0119	5.43	0.24
HQ1403_22/2	Rim	0.00201595	0.0089	5.36	0.18
<b>Median ± 2SD</b>				<b>5.42</b>	<b>0.30</b>

<b>AG1308A (n=20)</b>					
AG1308A_10/1	Core	0.00201590	0.0097	5.34	0.19
AG1308A_10/2	Rim	0.00201598	0.0103	5.38	0.21
AG1308A_17/1	Core	0.00201600	0.0077	5.39	0.15
AG1308A_17/2	Rim	0.00201626	0.0088	5.51	0.18
AG1308A_18/1	Core	0.00201613	0.0110	5.45	0.22
AG1308A_18/2	Rim	0.00201629	0.0086	5.53	0.17
AG1308A_2/1	Core	0.00201574	0.0086	5.26	0.17
AG1308A_2/2	Rim	0.00201582	0.0095	5.29	0.19
AG1308A_20/1	Core	0.00201581	0.0103	5.29	0.21
AG1308A_20/2	Rim	0.00201631	0.0096	5.54	0.19
AG1308A_3/1	Core	0.00201588	0.0111	5.33	0.22
AG1308A_3/2	Rim	0.00201589	0.0094	5.33	0.19
AG1308A_4/1	Core	0.00201597	0.0087	5.37	0.17
AG1308A_9/1	Core	0.00201558	0.0115	5.18	0.23
AG1308A_9/2	Rim	0.00201579	0.0089	5.28	0.18
AG1308A_5/1	Core	0.00201592	0.0090	5.35	0.18
AG1308A_6/1	Core	0.00201629	0.0073	5.53	0.15
AG1308A_6/2	Rim	0.00201630	0.0110	5.54	0.22
AG1308A_7/1	Core	0.00201653	0.0107	5.65	0.21
AG1308A_7/2	Rim	0.00201633	0.0095	5.55	0.19
<b>Median ± 2SD</b>				<b>5.37</b>	<b>0.25</b>
<b>VK1405 (n=20)</b>					
VK1405_10/1	Core	0.00201584	0.0085	5.31	0.17
VK1405_11/1	Core	0.00201592	0.0088	5.35	0.18
VK1405_11/2	Rim	0.00201581	0.0120	5.29	0.24
VK1405_16/1	Core	0.00201535	0.0095	5.06	0.19
VK1405_4/1	Core	0.00201566	0.0093	5.21	0.19
VK1405_4/2	Rim	0.00201564	0.0091	5.20	0.18
VK1405_5/1	Core	0.00201598	0.0084	5.38	0.17
VK1405_5/2	Intermediate	0.00201560	0.0101	5.19	0.20
VK1405_5/3	Rim	0.00201527	0.0136	5.02	0.27
VK1405_8/1	Core	0.00201569	0.0090	5.23	0.18
VK1405_9/1	Core	0.00201589	0.0108	5.33	0.22
VK1405_9/2	Rim	0.00201577	0.0099	5.27	0.20
VK1405_1/1	Core	0.00201571	0.0099	5.24	0.20
VK1405_23/1	Core	0.00201571	0.0095	5.24	0.19
VK1405_23/2	Rim	0.00201636	0.0114	5.57	0.23
VK1405_14/1	Core	0.00201562	0.0093	5.20	0.19
VK1405_15/1	Core	0.00201603	0.0081	5.40	0.16
VK1405_20/1	Core	0.00201574	0.0128	5.26	0.26
VK1405_13/1	Core	0.00201596	0.0128	5.37	0.26
VK1405_27/1	Core	0.00201592	0.0096	5.35	0.19
<b>Median ± 2SD</b>				<b>5.26</b>	<b>0.24</b>
<b>MR1403 (n=20)</b>					
MR1403_1/1	Core	0.00201637	0.0090	5.57	0.18
MR1403_1/2	Rim	0.00201610	0.0082	5.44	0.16
MR1403_10/1	Core	0.00201655	0.0092	5.66	0.18
MR1403_11/1	Core	0.00201628	0.0090	5.53	0.18
MR1403_11/2	Rim	0.00201632	0.0092	5.54	0.18
MR1403_12/1	Core	0.00201655	0.0114	5.66	0.23
MR1403_12/2	Rim	0.00201671	0.0090	5.74	0.18
MR1403_13/1	Core	0.00201640	0.0092	5.59	0.18
MR1403_13/2	Rim	0.00201623	0.0084	5.50	0.17
MR1403_19/1	Core	0.00201611	0.0090	5.44	0.18
MR1403_2/1	Core	0.00201622	0.0090	5.50	0.18
MR1403_2/2	Rim	0.00201610	0.0103	5.44	0.21
MR1403_3/1	Core	0.00201635	0.0084	5.56	0.17
MR1403_21/1	Core	0.00201647	0.0100	5.62	0.20
MR1403_21/2	Rim	0.00201639	0.0085	5.58	0.17
MR1403_6/1	Core	0.00201641	0.0094	5.59	0.19
MR1403_6/2	Rim	0.00201645	0.0077	5.61	0.15
MR1403_7/1	Core	0.00201613	0.0093	5.45	0.19
MR1403_8/1	Core	0.00201664	0.0088	5.71	0.18
MR1403_9/1	Core	0.00201661	0.0076	5.69	0.15
<b>Median ± 2SD</b>				<b>5.58</b>	<b>0.18</b>

| | | | |

<b>LI1303A1 (n=20)</b>					
LI1303A1_2/1	Core	0.00201650	0.0079	5.63	0.16
LI1303A1_2/2	Intermediate	0.00201634	0.0109	5.56	0.22
LI1303A1_2/3	Rim	0.00201648	0.0088	5.62	0.18
LI1303A1_3/1	Core	0.00201639	0.0094	5.58	0.19
LI1303A1_3/2	Rim	0.00201634	0.0084	5.55	0.17
LI1303A1_5/1	Core	0.00201657	0.0119	5.67	0.24
LI1303A1_5/2	Rim	0.00201640	0.0086	5.58	0.17
LI1303A1_6/1	Core	0.00201655	0.0107	5.66	0.21
LI1303A1_6/2	Rim	0.00201652	0.0099	5.64	0.20
LI1303A1_7/1	Core	0.00201668	0.0091	5.73	0.18
LI1303A1_7/2	Rim	0.00201668	0.0088	5.73	0.18
LI1303A1_8/1	Core	0.00201639	0.0118	5.58	0.24
LI1303A1_12/1	Core	0.00201658	0.0104	5.67	0.21
LI1303A1_12/2	Rim	0.00201647	0.0090	5.62	0.18
LI1303A1_15/1	Core	0.00201633	0.0073	5.55	0.15
LI1303A1_16/1	Core	0.00201671	0.0090	5.74	0.18
LI1303A1_17/1	Core	0.00201639	0.0108	5.58	0.22
LI1303A1_18/1	Core	0.00201655	0.0073	5.66	0.15
LI1303A1_19/1	Core	0.00201680	0.0081	5.79	0.16
LI1303A1_19/2	Rim	0.00201657	0.0114	5.67	0.23
<b>Median ± 2SD</b>				<b>5.64</b>	<b>0.14</b>
<b>KJ1207 (n=20)</b>					
KJ1207_1/1	Core	0.00201657	0.0113	5.67	0.23
KJ1207_1/2	Intermediate	0.00201647	0.0089	5.62	0.18
KJ1207_1/3	Rim	0.00201631	0.0078	5.54	0.16
KJ1207_10/1	Core	0.00201597	0.0120	5.37	0.24
KJ1207_10/2	Rim	0.00201574	0.0103	5.26	0.21
KJ1207_2/1	Core	0.00201597	0.0100	5.37	0.20
KJ1207_2/2	Rim	0.00201638	0.0086	5.58	0.17
KJ1207_3/1	Core	0.00201630	0.0107	5.53	0.21
KJ1207_3/2	Rim	0.00201629	0.0077	5.53	0.15
KJ1207_5/1	Core	0.00201609	0.0090	5.43	0.18
KJ1207_5/2	Rim	0.00201580	0.0088	5.28	0.18
KJ1207_7/1	Core	0.00201637	0.0080	5.57	0.16
KJ1207_12/1	Core	0.00201589	0.0100	5.33	0.20
KJ1207_14/1	Core	0.00201624	0.0085	5.50	0.17
KJ1207_16/1	Core	0.00201635	0.0089	5.56	0.18
KJ1207_17/1	Core	0.00201605	0.0097	5.41	0.19
KJ1207_17/2	Rim	0.00201561	0.0082	5.19	0.16
KJ1207_4/1	Core	0.00201619	0.0073	5.48	0.15
KJ1207_9/1	Core	0.00201654	0.0091	5.66	0.18
KJ1207_9/2	Rim	0.00201627	0.0097	5.52	0.19
<b>Median ± 2SD</b>				<b>5.51</b>	<b>0.27</b>

<b>KJ1002 (n=21)</b>					
KJ1002_1/1	Core	0.00201635	0.0095	5.56	0.19
KJ1002_1/2	Rim	0.00201594	0.0092	5.35	0.18
KJ1002_11/1	Core	0.00201569	0.0087	5.23	0.17
KJ1002_11/2	Rim	0.00201557	0.0089	5.17	0.18
KJ1002_16/1	Core	0.00201572	0.0098	5.24	0.20
KJ1002_16/2	Intermediate	0.00201615	0.0086	5.46	0.17
KJ1002_16/3	Rim	0.00201607	0.0100	5.42	0.20
KJ1002_2/1	Core	0.00201639	0.0092	5.58	0.18
KJ1002_2/2	Rim	0.00201616	0.0078	5.47	0.16
KJ1002_3/1	Core	0.00201663	0.0101	5.70	0.20
KJ1002_3/2	Rim	0.00201632	0.0093	5.55	0.19
KJ1002_6/1	Core	0.00201576	0.0098	5.27	0.20
KJ1002_6/2	Intermediate	0.00201573	0.0130	5.25	0.26
KJ1002_6/3	Rim	0.00201604	0.0093	5.41	0.19
KJ1002_9/1	Core	0.00201650	0.0086	5.64	0.17
KJ1002_9/2	Rim	0.00201625	0.0095	5.51	0.19
KJ1002_18/1	Core	0.00201653	0.0083	5.65	0.17
KJ1002_18/2	Rim	0.00201612	0.0094	5.45	0.19
KJ1002_24/1	Core	0.00201649	0.0092	5.63	0.18
KJ1002_24/2	Intermediate	0.00201617	0.0094	5.47	0.19
KJ1002_24/3	Rim	0.00201631	0.0093	5.54	0.19
<b>Median ± 2SD</b>				<b>5.47</b>	<b>0.31</b>
<b>KJ1316 (n=19)</b>					
KJ1316_1/1	Core	0.00201653	0.0078	5.65	0.16
KJ1316_13/1	Core	0.00201642	0.0093	5.59	0.19
KJ1316_14/1	Core	0.00201654	0.0121	5.66	0.24
KJ1316_14/2	Rim	0.00201644	0.0085	5.61	0.17
KJ1316_16/1	Core	0.00201666	0.0081	5.71	0.16
KJ1316_2/1	Core	0.00201602	0.0113	5.40	0.23
KJ1316_2/2	Rim	0.00201635	0.0108	5.56	0.22
KJ1316_4/1	Core	0.00201676	0.0102	5.76	0.20
KJ1316_4/2	Rim	0.00201647	0.0087	5.62	0.17
KJ1316_5/1	Core	0.00201638	0.0092	5.58	0.18
KJ1316_9/1	Core	0.00201696	0.0095	5.86	0.19
KJ1316_9/2	Rim	0.00201672	0.0084	5.75	0.17
KJ1316_18/1	Core	0.00201689	0.0082	5.83	0.16
KJ1316_18/2	Rim	0.00201648	0.0095	5.62	0.19
KJ1316_20/1	Core	0.00201673	0.0086	5.75	0.17
KJ1316_21/1	Core	0.00201659	0.0086	5.68	0.17
KJ1316_23/1	Core	0.00201634	0.0098	5.56	0.20
KJ1316_6/1	Core	0.00201640	0.0090	5.58	0.18
KJ1316_7/1	Core	0.00201643	0.0089	5.60	0.18
<b>Median ± 2SD</b>				<b>5.62</b>	<b>0.22</b>

<b>KJ1302A (n=20)</b>					
KJ1302A_13/1	Core	0.00201648	0.0125	5.63	0.25
KJ1302A_13/2	Rim	0.00201663	0.0097	5.70	0.19
KJ1302A_2/1	Core	0.00201640	0.0107	5.58	0.21
KJ1302A_2/2	Rim	0.00201651	0.0091	5.64	0.18
KJ1302A_3/1	Core	0.00201631	0.0075	5.54	0.15
KJ1302A_3/2	Rim	0.00201607	0.0089	5.42	0.18
KJ1302A_4/1	Core	0.00201635	0.0085	5.56	0.17
KJ1302A_4/2	Rim	0.00201618	0.0116	5.48	0.23
KJ1302A_5/1	Core	0.00201640	0.0111	5.58	0.22
KJ1302A_5/2	Rim	0.00201628	0.0089	5.52	0.18
KJ1302A_6/1	Core	0.00201623	0.0087	5.50	0.17
KJ1302A_7/1	Core	0.00201637	0.0102	5.57	0.20
KJ1302A_14/1	Core	0.00201630	0.0087	5.53	0.17
KJ1302A_16/1	Core	0.00201643	0.0097	5.60	0.19
KJ1302A_17/1	Core	0.00201636	0.0106	5.57	0.21
KJ1302A_19/1	Core	0.00201583	0.0087	5.30	0.17
KJ1302A_19/2	Rim	0.00201582	0.0086	5.29	0.17
KJ1302A_8/1	Core	0.00201627	0.0101	5.52	0.20
KJ1302A_9/1	Core	0.00201620	0.0092	5.49	0.18
KJ1302A_9/2	Rim	0.00201620	0.0099	5.49	0.20
<b>Median ± 2SD</b>				<b>5.54</b>	<b>0.20</b>
<b>KJ1324A (n=20)</b>					
KJ1324A_1/1	Core	0.00201712	0.0097	5.94	0.19
KJ1324A_1/2	Rim	0.00201689	0.0075	5.83	0.15
KJ1324A_10/1	Core	0.00201709	0.0122	5.93	0.24
KJ1324A_10/2	Rim	0.00201701	0.0105	5.89	0.21
KJ1324A_17/1	Core	0.00201686	0.0092	5.82	0.18
KJ1324A_17/2	Intermediate	0.00201713	0.0095	5.95	0.19
KJ1324A_17/3	Rim	0.00201689	0.0101	5.83	0.20
KJ1324A_4/1	Core	0.00201729	0.0084	6.03	0.17
KJ1324A_4/2	Rim	0.00201692	0.0095	5.84	0.19
KJ1324A_5/1	Core	0.00201741	0.0089	6.09	0.18
KJ1324A_5/2	Rim	0.00201708	0.0076	5.92	0.15
KJ1324A_8/1	Core	0.00201694	0.0115	5.86	0.23
KJ1324A_8/2	Rim	0.00201692	0.0093	5.84	0.19
KJ1324A_9/1	Core	0.00201692	0.0086	5.84	0.17
KJ1324A_16/1	Core	0.00201719	0.0110	5.98	0.22
KJ1324A_16/2	Rim	0.00201714	0.0086	5.95	0.17
KJ1324A_18/1	Core	0.00201708	0.0082	5.92	0.16
KJ1324A_18/2	Rim	0.00201698	0.0085	5.88	0.17
KJ1324A_22/1	Core	0.00201719	0.0103	5.98	0.21
KJ1324A_22/2	Rim	0.00201727	0.0098	6.02	0.20
<b>Median ± 2SD</b>				<b>5.92</b>	<b>0.15</b>



<b>LI1301 (n=20)</b>					
LI1301_11/1	Core	0.00201661	0.0082	5.69	0.16
LI1301_2/1	Core	0.00201725	0.0106	6.01	0.21
LI1301_2/2	Intermediate	0.00201732	0.0097	6.04	0.19
LI1301_2/3	Rim	0.00201684	0.0075	5.81	0.15
LI1301_3/1	Core	0.00201682	0.0086	5.79	0.17
LI1301_3/2	Rim	0.00201706	0.0100	5.91	0.20
LI1301_4/1	Core	0.00201735	0.0095	6.06	0.19
LI1301_4/2	Rim	0.00201744	0.0094	6.10	0.19
LI1301_5/1	Core	0.00201719	0.0090	5.98	0.18
LI1301_5/2	Rim	0.00201684	0.0085	5.81	0.17
LI1301_8/1	Core	0.00201708	0.0099	5.93	0.20
LI1301_15/1	Core	0.00201732	0.0117	6.04	0.23
LI1301_16/1	Core	0.00201716	0.0088	5.96	0.18
LI1301_16/2	Intermediate	0.00201708	0.0102	5.93	0.20
LI1301_16/3	Rim	0.00201697	0.0076	5.87	0.15
LI1301_17/1	Core	0.00201740	0.0094	6.08	0.19
LI1301_21/1	Core	0.00201712	0.0092	5.94	0.18
LI1301_21/2	Rim	0.00201721	0.0104	5.99	0.21
LI1301_6/1	Core	0.00201722	0.0090	6.00	0.18
LI1301_6/2	Rim	0.00201728	0.0095	6.03	0.19
<b>Median ± 2SD</b>				<b>5.97</b>	<b>0.22</b>

**Standard**

S0081\_UAMT 0.00201497 4.87

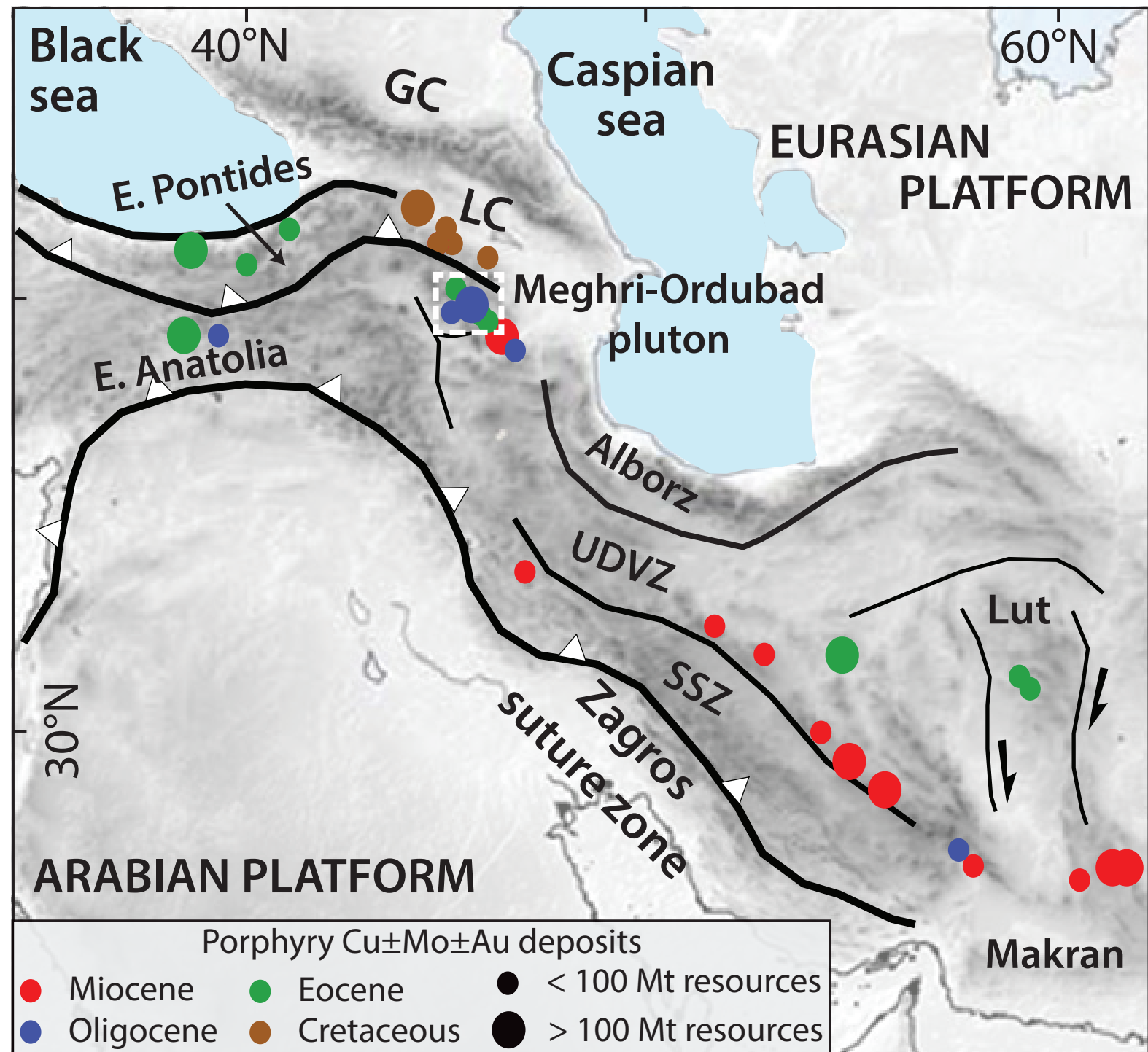


Figure DR1: Distribution of porphyry Cu±Mo±Au deposits grouped by ages and sizes along the Afro-Arabian collision zone located in the central Tethyan metallogenic belt. Locations and ages of porphyry deposits are derived principally from Singer et al. (2008), with updated information from Aghazadeh et al. (2015) and Richards (2015). Suture zones and structures are derived from Mouthereau et al. (2012) and the topographic relief background map from ETOPO1 (1'×1' resolution) Global Relief data (<http://www.ngdc.noaa.gov>). Abbreviations are Greater Caucasus (GC), Lesser Caucasus (LC), Sanandaj-Sirjan Zone (SSZ) and Urumieh-Dokhtar Volcanic Zone (UDVZ).

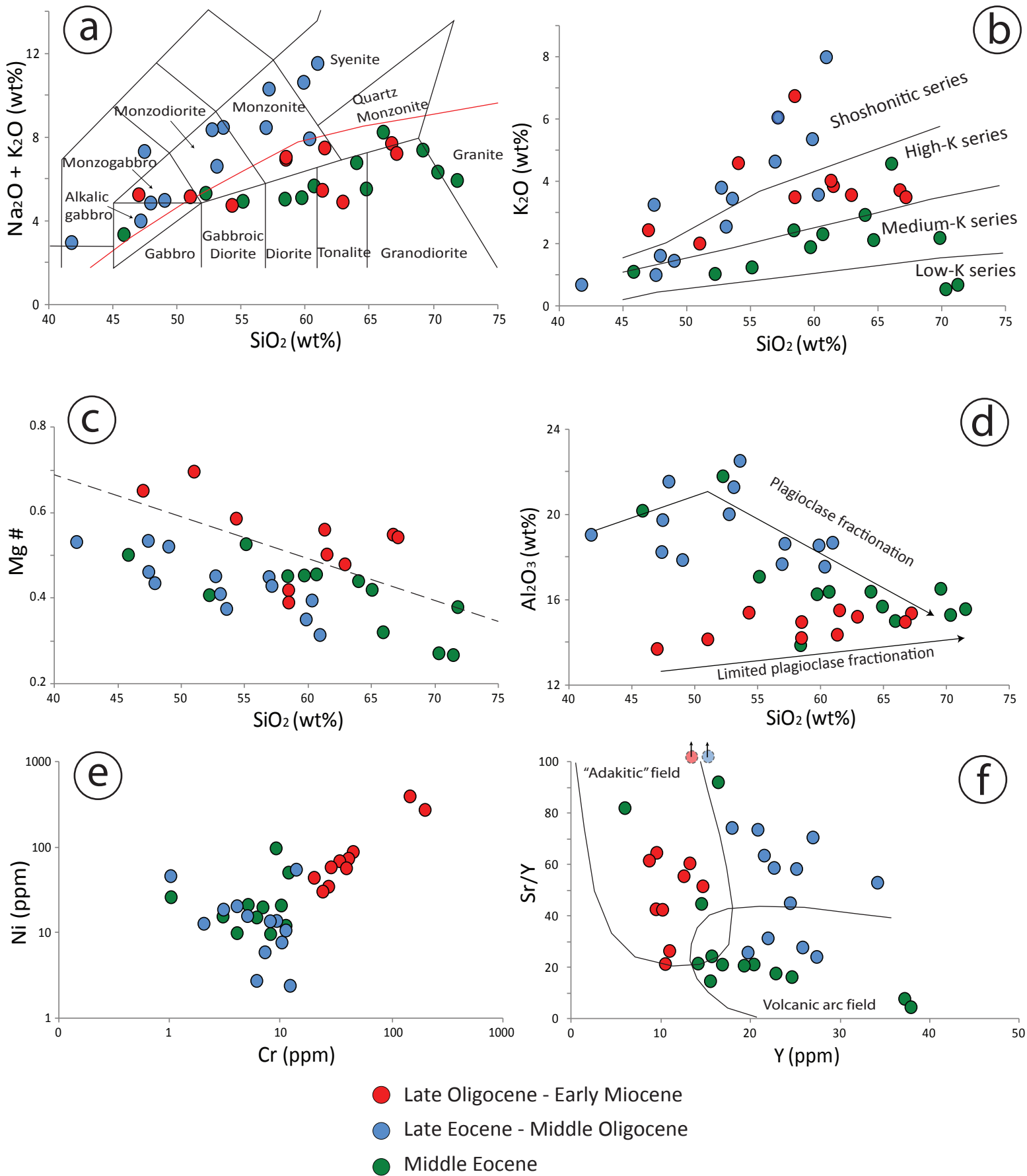


Figure DR2: a) Total Alkali Silica (TAS) diagram (Le Maître et al., 1989). b)  $\text{K}_2\text{O}$  vs.  $\text{SiO}_2$  Harker diagram (Pecorillo and Taylor, 1976). c)  $\text{Mg\#}$  vs.  $\text{SiO}_2$  Harker diagram. d)  $\text{Al}_2\text{O}_3$  vs.  $\text{SiO}_2$  Harker diagram. e) Ni vs. Cr. f) Sr/Y vs. Y.

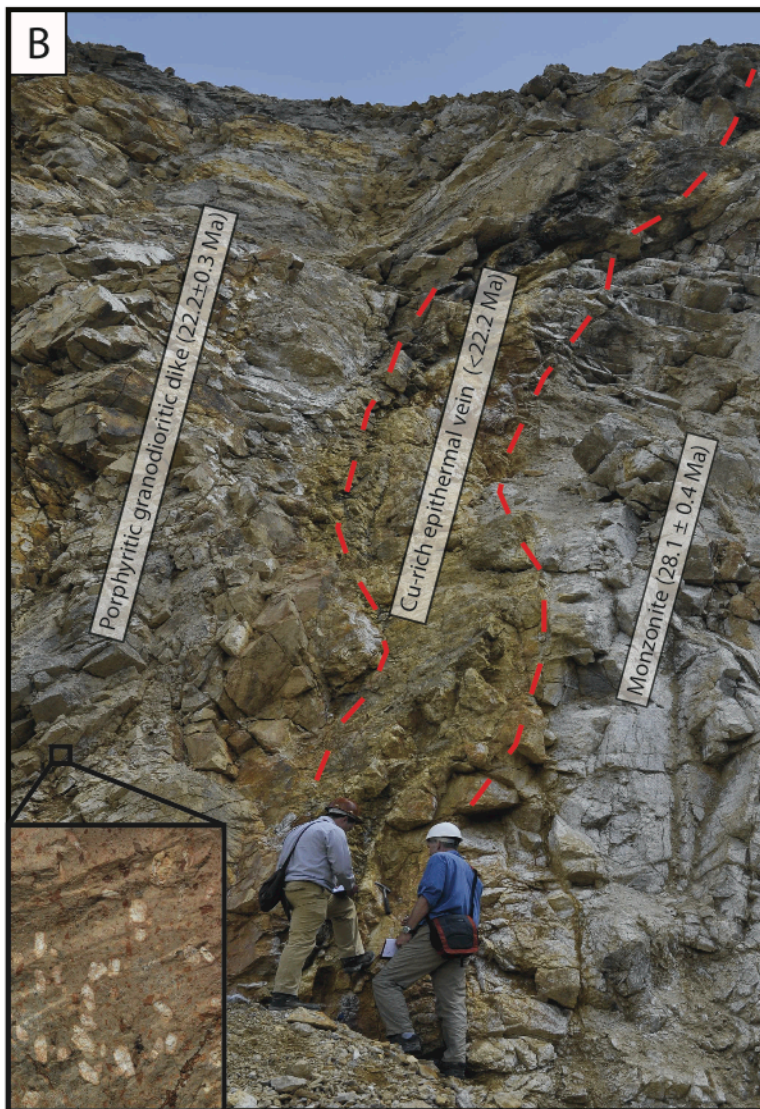
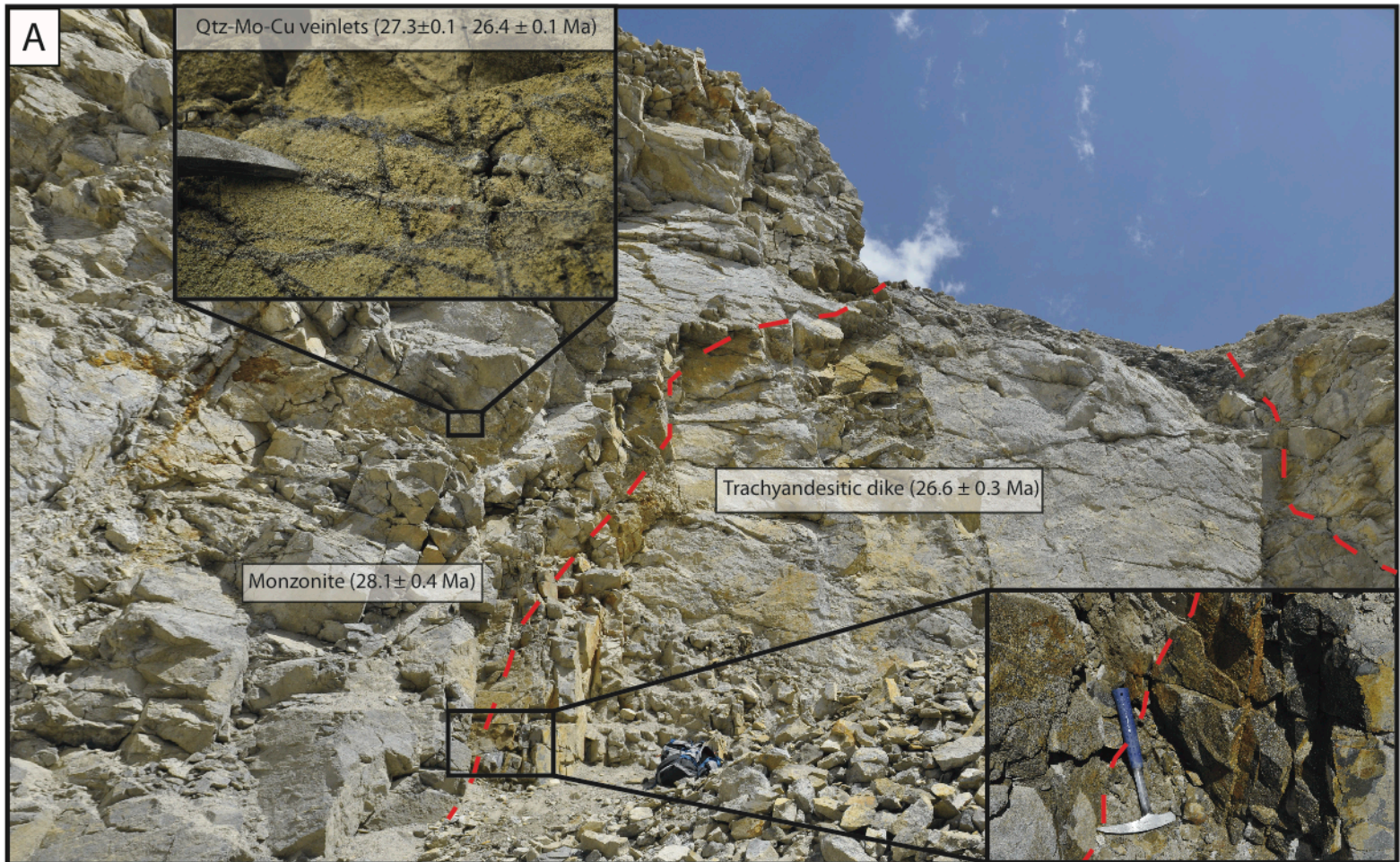


Figure DR3: A) Crosscutting relationships between the monzonite-bearing mineralization and the trachyandesitic dike. B) Crosscutting relationships showing a Cu-rich epithermal vein crosscutting the altered monzonite (propylitic, potassic) and creating an important hydrothermal alteration (kaolinitisation, silicification) of the porphyritic granodioritic dike.

## REFERENCES

- Aghazadeh, M., Hou, Z., Badrzadeh, Z., and Zhou, L., 2015, Temporal–spatial distribution and tectonic setting of porphyry copper deposits in Iran: Constraints from zircon U–Pb and molybdenite Re–Os geochronology: *Ore Geology Reviews*, v. 70, p. 385-406, doi:10.1016/j.oregeorev.2015.03.003.
- Le Maitre, R. W. B., Dudek, P., Keller, A., Lameyre, J., Le Bas, J., Sabine, M.J., Schmid, P.A., Sorensen, R., Streckeisen, H., Woolley, A. and Zanettin, A.R., 1989, A classification of igneous rocks and glossary of terms: Recommendations of the International Union of Geological Sciences, Subcommission on the Systematics of Igneous Rocks: Blackwell Scientific Publications, Oxford, 193 p.
- Mouthereau, F., Lacombe, O. and Vergés, J., 2012, Building the Zagros collisional orogen: timing, strain distribution and the dynamics of Arabia/Eurasia plate convergence: *Tectonophysics*, v. 532, p. 27-60, doi:10.1016/j.tecto.2012.01.022.
- Pecerillo, A., and Taylor, S.R., 1976, Geochemistry of Eocene calc-alkaline volcanic rocks from the Kastamanou area, northern Turkey: *Contributions to Mineralogy and Petrology*, v. 58, p. 63–81, doi: 10.1007/BF00384745.
- Richards, J.P., 2015, Tectonic, magmatic, and metallogenic evolution of the Tethyan orogen: from subduction to collision: *Ore Geology Review*, v. 70, p. 323-345, doi: 10.1016/j.oregeorev.2014.11.009.
- Singer, D. A., Berger, V. I., Moring, B. C., 2008, Porphyry copper deposits of the world: database and grade and tonnage models: U.S. Geological Survey Open-File Report 2008-1155, 45 p. (<http://pubs.usgs.gov/of/2008/1155/>).